

The metal-binding GTPases CobW2 and CobW3 are at the crossroads of zinc and cobalt homeostasis in *Cupriavidus metallidurans*

Diana Galea,¹ Martin Herzberg,^{1,2} Dietrich H. Nies¹

AUTHOR AFFILIATIONS See affiliation list on p. 25.

ABSTRACT The metal-resistant beta-proteobacterium *Cupriavidus metallidurans* is also able to survive conditions of metal starvation. We show that zinc-starved cells can substitute some of the required zinc with cobalt but not with nickel ions. The zinc importer ZupT was necessary for this process but was not essential for either zinc or cobalt import. The cellular cobalt content was also influenced by the two COG0523-family proteins, CobW2 and CobW3. Pulse-chase experiments with radioactive and isotope-enriched zinc demonstrated that both proteins interacted with ZupT to control the cellular flow-equilibrium of zinc, a central process of zinc homeostasis. Moreover, an antagonistic interplay of CobW2 and CobW3 in the presence of added cobalt caused a growth defect in mutant cells devoid of the cobalt efflux system DmeF. Full cobalt resistance also required a synergistic interaction of ZupT and DmeF. Thus, the two transporters along with CobW2 and CobW3 interact to control cobalt homeostasis in a process that depends on zinc availability. Because ZupT, CobW2, and CobW3 also direct zinc homeostasis, this process links the control of cobalt and zinc homeostasis, which subsequently protects *C. metallidurans* against cadmium stress and general metal starvation.

IMPORTANCE In bacterial cells, zinc ions need to be allocated to zinc-dependent proteins without disturbance of this process by other transition metal cations. Under zinc-starvation conditions, *C. metallidurans* floods the cell with cobalt ions, which protect the cell against cadmium toxicity, help withstand metal starvation, and provide cobalt to metal-promiscuous paralogs of essential zinc-dependent proteins. The number of cobalt ions needs to be carefully controlled to avoid a toxic cobalt overload. This is accomplished by an interplay of the zinc importer ZupT with the COG0523-family proteins, CobW3, and CobW2. At high external cobalt concentrations, this trio of proteins additionally interacts with the cobalt efflux system, DmeF, so that these four proteins form an inextricable link between zinc and cobalt homeostasis.

KEYWORDS zinc, cobalt, *Cupriavidus metallidurans*

Cupriavidus metallidurans is a beta-proteobacterium that is adapted to metal-rich environments such as zinc deserts and auriferous soils (1–4). *C. metallidurans* strain CH34 contains a chromosome, a chromid, and two large plasmids with a variety of metal-resistance determinants (5, 6). The gene products of these determinants export excessively high concentrations of transition metal ions from the cytoplasm to the periplasm, and others from there to the outside. In the case of some metals, reduction and oxidation reactions to less toxic species are also mechanisms employed to decrease the toxic burden of the respective metal ion or complex (7).

Editor Conrad W. Mullineaux, Queen Mary University of London, London, United Kingdom

Address correspondence to Dietrich H. Nies, d.nies@mikrobiologie.uni-halle.de.

The authors declare no conflict of interest.

See the funding table on p. 25.

Received 31 May 2024

Accepted 3 July 2024

Published 23 July 2024

Copyright © 2024 Galea et al. This is an open-access article distributed under the terms of the [Creative Commons Attribution 4.0 International license](https://creativecommons.org/licenses/by/4.0/).

Cobalt and zinc ions can be imported into the *C. metallidurans* cell by a variety of import systems (8–10), for instance, secondary, *proton motive force*-driven members ZupT of the ZIP [ZRT/IRT, TC2.A.5 (11, 12)] and CorA1, CorA2, and CorA3 of the MIT (metal inorganic transport, TC1.A.35) families. The name of these latter transport systems stems from the fact that a deletion of the cognate gene results in increased cobalt tolerance (13, 14). When the cytoplasmic content of zinc or cobalt ions becomes too high, Zn(II) is exported by the P_{IB2}-type ATPases ZntA and CadA, and Co(II) is exported by the CDF (cation diffusion facilitator, TC2.A.4) protein, DmeF (Fig. S1) (15, 16). At even higher concentrations of these ions, the plasmid-encoded transenvelope efflux systems CzcCBA and CnrCBA export Zn(II) and Co(II) to the environment (7). Thus, export and import reactions adjust the cytoplasmic metal zinc concentration in a flow equilibrium, which is buffered by cytoplasmic metal-binding activities (17, 18). The expression “flow equilibrium” was used here to emphasize the importance of metal transport systems to reach the steady state condition of cellular zinc homeostasis.

Despite being a metal-resistant bacterium, *C. metallidurans* is also able to cope with metal-starvation conditions. In the case of zinc ion limitation, the Zur regulon mediates this ability (19–21). Products of this regulon are Zur itself, ZupT, and two metal-binding GTPases of the COG0523 family (20–24), CobW2 and CobW3 (Fig. S1). CobW2 is a zinc-storage compound that binds up to six Zn ions per polypeptide with low affinity at binding sites in the middle of the peptide chain and can unfold in the presence of MgGTP. CobW3 has no a GTPase activity but is able to sequester up to eight Zn ions per polypeptide with decreasing affinity to sites located at the carboxy terminus and equilibrates metal import by ZupT with that of other metal transport systems. When treated with a mixture of metal ions, CobW3 is also able to bind 2 Ni(II), 1 Co(II), and 1 Cd(II) instead of four Zn ions (20). Moreover, under even more extreme zinc starvation conditions, release of Zur from a double binding site at the *cobW1p* promoter allows expression of an operon encoding CobW1 as a third CobW protein, along with several paralogs of zinc-requiring enzymes and the metal-promiscuous GTP cyclohydrolyase Fole_IB2 (20, 21, 25). Fole-type enzymes are important for the initiation of folate biosynthesis by cyclo-hydrolyzation of GTP, and synthesis of GTP needs tetrahydrofolate; hence, folate biosynthesis can be described as an “Achilles heel” of bacterial metabolism (26–28).

C. metallidurans possesses three Fole-type enzymes, the strictly zinc-dependent Fole_IA, and the metal-promiscuous Fole_IB1 and Fole_IB2 proteins. Fole_IB1 and IB2 are needed for growth under zinc-starvation conditions (25). The optimally suited cofactors for the two Fole_IBs are Fe(II), Mn(II), and Co(II) (25); however, *C. metallidurans* contains only a very low number of Mn atoms per cell, does not have a NRAMP-type manganese importer (TC2.A.55), and lacks a Mn-dependent superoxide dismutase (8, 29). Iron, on the other hand, is used for a multitude of biochemical reactions (30), but uncontrolled Fe(II) can be extremely detrimental due to its ability to catalyze the Fenton reaction (31–33).

This leaves Co(II) as the most suitable metal cofactor for the metal-promiscuous enzymes in *C. metallidurans* under zinc starvation conditions, besides cobalamin as an important cobalt sink (34). Nevertheless, too high intracellular cobalt concentrations are toxic and damage-nascent iron-sulfur clusters (35–37). If Co(II) can substitute for Zn(II), as discussed for *Salmonella* (38), it should be used only under zinc starvation conditions, and its cellular content must be strictly controlled. In addition to the overall affinity of a metal cation to a protein as defined by its rank in the Irving-Williams series (39), the actual availability controls metalation of a protein by a specific metal cation in competition with another metal cation (40, 41). Although CobW2 has been discussed to be a zinc-storing protein, CobW3 may be capable of sensing metal availability by binding the cations at its carboxy-terminal metal-binding site and use this information to control metal homeostasis by influencing activity of metal transport systems. It is therefore conceivable that the actual availability of cobalt and zinc could control metalation of CobW3 and, subsequently, the import of zinc and other metal cations.

This current study provides evidence for three processes that support the above proposal. First, *C. metallidurans* fills up a part of its cellular zinc pool with cobalt ions. ZupT and CobW3 control this response with a minor contribution from CobW2. Second, these three proteins are also involved in the cellular flow equilibrium of zinc by affecting zinc import rather than efflux. Third, disturbance of the zinc-cobalt homeostasis mediated by these three proteins results in decreased cobalt, cadmium, and metal-starvation tolerance, with DmeF supporting ZupT, CobW3, and CobW2 (Fig. S1) to mediate cobalt resistance.

RESULTS

Experimental strategy

Due to the fact that the GTP cyclohydrolase FolE_IB1 can be activated by Co(II) 50-times more effectively than by Ni(II) (25), *C. metallidurans* may import cobalt rather than nickel under zinc starvation conditions to metalate this enzyme and continue folate biosynthesis. To investigate whether zinc availability influences the cellular cobalt content, the cells were cultivated in Tris-buffered mineral salts medium TMM (5) with gluconate as the carbon source but with different zinc and cobalt concentrations (Table S1). In TMM, trace element solution SL6 (42) provided 35.3 nM Zn(II) and 84.1 nM Co(II) to the medium; however, the actual zinc content varies due to the zinc content of the respective NaSO₄ source (25). This fact was used to design six TMM solutions with different zinc and cobalt concentrations exposing the *C. metallidurans* cells to different levels of zinc and cobalt starvation stress (Table S1). All strains used (Table S2) were derivatives of the plasmid-free strain AE104 because a $\Delta zupT$ deletion results in curing of the plasmid pMOL30 in *C. metallidurans* CH34 wild type (43). All experiments were performed at least as three biological repeats. For most experiments, data points were judged as different if their ratio was at least two and if their deviation bars did not touch or overlap.

Zinc controls cobalt homeostasis in *C. metallidurans*

C. metallidurans strain AE104 was cultivated to the mid-exponential phase of growth (150 Klett units) in three TMM media with 200 nM (aZn), 64 nM (mZn), or 39 nM (lZn) Zn(II), respectively (Table 1). As determined by ICP-MS (inductively coupled plasma mass spectrometry), the zinc content of the cells decreased with the decreasing zinc content of the respective medium from 101,000 Zn per cell via 33,000 down to 7,100 when no

TABLE 1 Metal content of *C. metallidurans* strain AE104 in different TMM media^a

Addition	Atoms per cell						
	Mg, 10 ⁶	Ca, 10 ³	Fe, 10 ³	Zn, 10 ³	Co, 10 ³	Ni, 10 ³	Cu, 10 ³
TMM 200 nM Zn (aZn)							
0 μM Zn	13.4 ± 0.7	251 ± 9	998 ± 4	101 ± 4	5.3 ± 0.4	4.2 ± 0.2	5.6 ± 0.4
1 μM Zn	14.8 ± 0.6	231 ± 27	1,082 ± 14	128 ± 8	4.7 ± 0.3	4.4 ± 0.2	4.7 ± 0.2
10 μM Zn	14.1 ± 0.3	197 ± 18	1,059 ± 33	124 ± 4	4.4 ± 0.2	4.0 ± 0.0	4.7 ± 0.3
100 μM Zn	17.6 ± 0.4	139 ± 8	834 ± 37	157 ± 19	4.4 ± 0.0	3.4 ± 0.0	5.1 ± 0.2
TMM 64 nM Zn(II) (mZn)							
0 μM Zn	11.2 ± 0.3	269 ± 166	819 ± 28	33.4 ± 5.4	20.5 ± 0.9	5.0 ± 0.6	4.3 ± 0.7
1 μM Zn	11.9 ± 0.2	280 ± 131	874 ± 10	115 ± 1	18.4 ± 1.6	3.6 ± 0.4	4.2 ± 0.4
10 μM Zn	12.6 ± 0.4	209 ± 74	863 ± 33	160 ± 4	21.4 ± 1.3	3.9 ± 0.2	4.1 ± 0.3
100 μM Zn	14.3 ± 0.5	120 ± 66	641 ± 19	155 ± 10	17.7 ± 0.7	2.8 ± 0.3	4.3 ± 1.1
TMM 39 nM Zn(II), no SL6 (lZn)							
0 μM Zn	13.3 ± 0.4	193 ± 43	1,003 ± 40	7.1 ± 1.2	0.3 ± 0.0	4.2 ± 0.1	2.8 ± 0.6
1 μM Zn	13.0 ± 0.5	277 ± 98	850 ± 52	113 ± 8	0.2 ± 0.0	3.3 ± 0.2	5.3 ± 3.4
10 μM Zn	13.9 ± 0.6	187 ± 48	840 ± 45	138 ± 9	0.2 ± 0.0	3.1 ± 0.2	2.4 ± 0.2
100 μM Zn	16.6 ± 0.7	142 ± 43	709 ± 14	186 ± 18	0.2 ± 0.0	2.6 ± 0.1	2.8 ± 0.5

^a*C. metallidurans* AE104 was cultivated in TMM medium with ambient zinc (aZn) TMM, which leads to fully zinc-replete cells, under moderate zinc starvation (mZn) and under low zinc and cobalt (lZn) to a turbidity of 100 Klett, before mid-exponential phase of growth. Zn(II) was added at the indicated concentration. Incubation was continued with shaking to a turbidity of 150 Klett units reaching the mid-exponential phase and the metal content was determined by ICP-MS. *n* = 3, with the standard deviations indicated.

SL6 was added to the medium. When more zinc (1, 10, and 100 μM) was added to these cells before the mid-exponential phase of growth, their zinc content increased. At high zinc concentrations, the zinc ion content of the cells that had been cultivated under these conditions was similar and reached an intracellular saturation of the zinc repository with on average 150,000 Zn ions per cell, which is comparable with previous studies (17).

Although no important changes between the intracellular content of Mg, Ca, Fe, Ni, and Cu could be observed (Table 1), the cobalt content depended on the medium zinc or cobalt concentration. Cells grown in the presence of the same cobalt concentration (86 nM) with 200 nM (aZn) zinc contained $\sim 5,000$ Co ions per cell, but with 64 nM Zn (mZn) about 20,000, and those in low zinc and low cobalt (~ 2 nM) medium only a few hundred Co atoms per cell were detected. Addition of zinc (1, 10, or 100 μM) before reaching the mid-exponential phase of growth did not change the cobalt content of the cells in this incubation experiment in indirect proportion to the zinc content. The cells seemed to have accumulated more cobalt under zinc starvation condition (mZn) than under zinc-replete conditions (aZn), provided sufficient cobalt (86 nM) was available in these growth media, which was not the case in media without SL6 (lZn) (Table 1). The threshold for the zinc concentration that stimulated increased cobalt accumulation should be between 64 nM and 200 nM Zn(II) but was far below 1 μM Zn(II). Zinc starvation controlled the cobalt level of the cells, but the starvation stress had to be present at the beginning of growth, or even in the pre-cultures. It took some time for the cells to experience starvation conditions and react to them.

To obtain a better measure for the threshold concentration of zinc that governs the cobalt level, strain AE104 was cultivated in standard TMM (160 nM Zn), high-zinc (400 nM Zn), and low zinc-cobalt medium (39 nM Zn) without trace element solution SL6 (Table 2). As published previously (8, 17, 21, 43, 44), the zinc content of the parental strain AE104 remained at about 70,000 to 80,000 Zn ions per cell in standard TMM, which included 160 nM Zn(II) (Table 2). The increased zinc concentration in high zinc medium

TABLE 2 Zinc and cobalt content of *C. metallidurans* strain AE104 and its ΔzupT mutant under various growth conditions^a

Strain	Medium		1,000 Metal atoms per cell	
	Zn (nM)	Co (nM)	Co	Zn
High-zinc TMM (hZn)				
AE104	400	110	3.7 \pm 1.1	75.8 \pm 7.7
ΔzupT	400	110	6.4 \pm 0.9	42.8 \pm 4.3
Standard TMM				
AE104	160	110	21.3 \pm 10.7	68.4 \pm 12.4
ΔzupT	160	110	7.3 \pm 1.9	28.6 \pm 4.8
Low-zinc-cobalt, no SL6 (lZn)				
AE104	39	2	0.153 \pm 0.045	27.5 \pm 11.0
AE104	39	100	40.2 \pm 3.6	18.1 \pm 9.6
AE104	39	150	40.0 \pm 7.4	19.7 \pm 5.8
AE104	39	300	57.2 \pm 16.5	21.6 \pm 8.7
AE104	190	100	25.6 \pm 3.6	83.6 \pm 6.1
AE104	190	150	20.6 \pm 3.5	65.4 \pm 4.7
AE104	190	300	24.9 \pm 3.2	74.5 \pm 8.2
ΔzupT	39	2	0.105 \pm 0.073	19.9 \pm 2.4
ΔzupT	39	100	35.2 \pm 3.3	14.6 \pm 2.2
ΔzupT	39	150	44.8 \pm 5.9	14.5 \pm 6.2
ΔzupT	39	300	46.5 \pm 19.8	37.1 \pm 8.5
ΔzupT	190	100	5.4 \pm 0.5	32.5 \pm 2.8
ΔzupT	190	150	8.2 \pm 0.8	23.3 \pm 3.5
ΔzupT	190	300	14.1 \pm 4.6	25.8 \pm 4.4

^aSame cultivation conditions as in Table 1. The metal content was verified by ICP-MS and was in the expected range. Data for all metals are presented in Table S3

with 400 nM Zn(II) did not change this number in AE104, although the deviation of this number decreased by half compared with the standard medium.

Again, strain AE104 accumulated approximately 20,000 Zn ions per cell in low Zn-Co medium (lZn) (Tables 1 and 2). This was not surprising because 39 ± 8 nM zinc in low zinc/cobalt medium was distributed among 1.2×10^{12} cells L^{-1} (around the mid-exponential phase of growth), resulting in a maximal number of $19,500 \pm 4,000$ Zn ions per cell. In low-zinc medium, the zinc content may have been exhausted after growth. A similar calculation for the zinc content of moderate zinc medium of 160 ± 36 nM distributed among the cells calculates to $80,000 \pm 18,000$ Zn ions per cell. Again, the zinc content of the zinc growth medium was mirrored by that of the cellular zinc content. In contrast, the cellular zinc content remained at 76,000 Zn ions per cell in high zinc medium (400 nM, Table 2). The cells limited their cellular zinc content, e.g., by ZntA-mediated zinc efflux. They were under zinc starvation in low Zn-Co medium, exactly at the edge of zinc starvation at 160 nM zinc but were supplied with sufficient zinc at 400 nM zinc in the medium (Table 2).

A complete distribution of the 2 nM cobalt ions in low zinc/cobalt medium would result in about 1,000 Co ions per cell. The cobalt content of these cells was even below this number (Table 2). In moderate and high zinc media, complete distribution of the approximately 100 nM Co would give 50,000 Co ions per cell. The measured level was below this number, about 21,000 Co ions per cell in moderate zinc and only about 3,700 Co ions per cell in high zinc medium. When on the verge of zinc starvation, the cells accumulated a higher number of Co ions; however, accumulation did not exhaust the cobalt content of the growth medium. Zinc availability in the growth medium did indeed prove to control the cellular cobalt content.

To test this observation further, strain AE104 was cultivated in TMM adjusted to concentrations between 85 nM and 300 nM Zn(II), and the metal content of medium and cells was determined by ICP-MS (Fig. 1A). The cellular zinc content increased with increasing metal availability and followed a curve that reached saturation at 150 nM Zn(II) in the growth medium. The cellular cobalt content, in contrast, followed an inverse

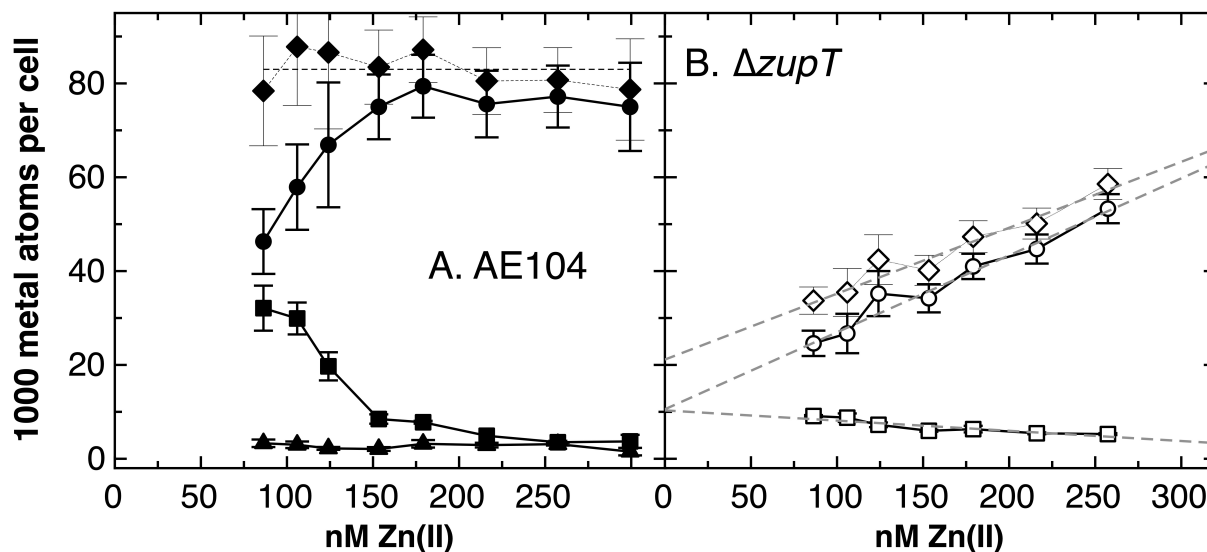


FIG 1 Zinc availability controls the cellular cobalt content in *C. metallidurans* AE104 and ZupT is required for this process. Cells were cultivated in moderate zinc mZn-TMM with an adjusted zinc content to the exponential phase of growth. The cellular zinc (circles), cobalt (squares), and nickel (triangles) contents were measured by ICP-MS. The diamonds represent the sum of the zinc plus cobalt contents per cell. Panel A. The *C. metallidurans* parental strain, AE104. The dashed line indicates the mean value of the sum of the zinc and cobalt content of $83,000 \pm 3,900$ (Zn + Co)/cell. Panel B. The cellular zinc content of the $\Delta zupT$ strain (open symbols) was fitted to the zinc availability with $11,300 \pm 2,500$ Zn/cell + 161 ± 15 zn/cell * nM medium zinc (98%), the cobalt content was $10,600 \pm 800$ Co/cell - 23 ± 5 Co/cell * nM medium zinc (91%), and the Zn + Co content was $21,100 \pm 3,900$ (Zn + Co)/cell + 140 ± 22 (Zn + Co)/cell * nM medium zinc (97%). These functions are shown with dashed gray lines.

curve. The sum of both metal contents was $83,000 \pm 3,900$ Zn + Co ions per cell. The cells filled up their cobalt content to a level of 83,000 ions per cell minus the zinc content. Interestingly, the nickel content of the cells was not affected (Fig. 1A, triangles). This demonstrated clearly that the zinc availability in the growth medium controlled the cobalt, but not the nickel, content in *C. metallidurans* strain AE104. This may allow cobalt ions to substitute for zinc ions and reflects a possible shared metal pool in the cell.

The zinc importer ZupT of the ZIP protein family is involved in zinc-mediated control of the cellular cobalt content

When the $\Delta zupT$ mutant was incubated in TMM with adapted zinc concentrations (Fig. 1B), the zinc content of the mutant cells was lower than that of the parent; it did not follow a saturation curve but followed a linear fashion with the zinc content of the medium exhibiting an increase of 161 ± 17 Zn ions per cell per nM exogenously supplied Zn. The cobalt content decreased with the zinc content of the medium, corresponding to a decrease in 23 ± 5 Co ions per cell per nM Zn in the growth medium. Both lines crossed the y-axis at $x = 0$ with similar numbers, $11,300 \pm 2,300$ Zn and $10,600 \pm 800$ Co ions per cell. The total zinc plus cobalt content increased such that 140 ± 22 (Zn + Co) ions per cell per nM Zn represented the sum for the zinc and cobalt ion content (Fig. 1B).

The zinc content of the $\Delta zupT$ mutant cultivated in moderate zinc and low zinc/cobalt medium (Table 2) was at a value that could be expected from the linear function of the ion (Fig. 1B). In high zinc medium, the cells contained only 42,800 Zn ions per cell, much less than expected from the linear function. This indicated that efflux systems had been activated, for instance, ZntA. Nevertheless, ZupT was also required to adjust the cellular zinc content in high zinc medium. The cobalt content was also at the level expected based on the linear function (Fig. 1B) or from an exhaustive accumulation of the available cobalt in low zinc/cobalt medium (Table 2).

For a more detailed characterization of the role of ZupT in cobalt accumulation, the $\Delta zupT$ strain and its parent AE104 were cultivated in low zinc-cobalt (lZn) medium, which was supplemented with 100 nM, 150 nM, or 300 nM cobalt chloride, with or without additional 150 nM zinc chloride. This resulted in zinc concentrations in the growth medium of 39 nM or 190 nM (Table 2). At 39 nM Zn(II) in the medium, the cellular zinc content remained at the expected 20,000 Zn ions per cell with no difference between the $\Delta zupT$ strain and its parent; all available zinc had been accumulated. When Co(II) was added to the cells, both strains accumulated between 37,000 and about 50,000 Co ions per cell at 100 nM, 150 nM, or 300 nM Co(II) (Table 2). Again, the absence of ZupT made no difference with respect to the cellular cobalt content, despite the presence of the remaining import systems for divalent metal cations in the *C. metallidurans* cell. The cobalt content of the medium was not exhausted, although the Zn + Co content of 83,000 ions per cell had not been reached. Strain AE104 substituted Co for Zn only to between 50% and 70% of the total of 83,000 Zn + Co ions, however, not completely. ZupT was not needed under zinc starvation conditions at 39 nM Zn(II) for exhaustive zinc accumulation.

At 190 nM Zn(II), the zinc content of the AE104 parental strain was saturated between 70,000 and 80,000 Zn ions per cell (Fig. 1A; Table 2) but that of the $\Delta zupT$ mutant accumulated only between 23,000 and 32,000 Zn ions per cell (Table 2). This level was expected based on the linear dependence of the Zn content of $\Delta zupT$ cells on the zinc availability (Fig. 1B). In contrast to the parental strain, the Co content of $\Delta zupT$ cells remained very low when Co(II) was added to this medium. The Co content in $\Delta zupT$ increased in a linear fashion with the cobalt content of the medium but only in the presence of sufficient zinc (Table 2).

Under all these conditions, the cellular content of Ca, Mn, Fe, and Mo remained unchanged with some minor deviations of the copper content (Table S3). The nickel content was decreased at high cobalt concentrations. The magnesium content was increased by a factor of three in the $\Delta zupT$ mutant when grown in low zinc/cobalt medium that was supplemented with exogenous zinc and cobalt.

The largest difference between the zinc and cobalt content of the $\Delta zupT$ mutant and its parent was visible in standard TMM without any additions (Table 2). When Co(II) was added (Table 3), strain AE104 did not increase its cellular cobalt content when 1 μM Co(II) was added, but the level increased 2.7-fold when 5 μM Co(II) was added. The $\Delta zupT$ mutant cells started from a lower cobalt level of 7,000 Co ions per cell when cultivated without added Co and the level increased 3.4-fold and 8.7-fold when 1 μM or 5 μM Co(II) was added, respectively. Thereby, the $\Delta zupT$ cells attained a similar Co content to the parent cells. The zinc content of these cells decreased 0.42-fold in the $\Delta zupT$ mutant compared with AE104 when the cells were cultivated without added cobalt and remained at this level when cobalt was added (Table S4).

CobW2 and CobW3 control cobalt homeostasis in *C. metallidurans*

In cells cultivated in standard TMM, the absence of the gene encoding CobW3 resulted in a strongly decreased cobalt content that was at a level of approximately 4,000 Co ions per cell, compared with 20,000 Co ions per cell in the parental strain, AE104 (Table 3). A mutant lacking CobW2 had 13,000 Co ions per cell after growth under the same conditions. A $\Delta cobW2 \Delta cobW3$ double null mutant did not decrease the Co content any further than what was measured in the $\Delta cobW3$ single null mutant (Table 3). When 1 μM Co(II) was added to the growth medium, the parental strain increased its cellular cobalt content only slightly. By contrast, compared with the non-amended medium, the three $\Delta cobW$ mutants increased their intracellular cobalt content between 1.8-fold to 4.5-fold (Table 3). When 5 μM Co(II) was added to the medium, all four strains attained similar cobalt levels of between 39,000 for the double null mutant and 55,000 Co ions per cell for the parental strain.

Deletion of $\Delta zupT$ resulted in a decreased cobalt content in the cells of 36%, and this decreased number of cobalt ions per cell was not affected by additional deletion of

TABLE 3 Cobalt content of mutant strains cultivated in standard TMM^a

Added Co(II), μM	0	1	5
Strains	1,000 Co per cell; Q (D)		
AE104	20.0 \pm 8.7 (1.00; 0.0)	24.1 \pm 2.0 (1.20; 0.4)	54.7 \pm 9.1 (2.73; 2.0)
$\Delta cobW3$	3.9 \pm 1.2 (0.19; 1.6)	14.9 \pm 2.4 (3.84; 3.1)	46.3 \pm 4.4 (11.9; 7.5)
$\Delta cobW2::dis$	13.3 \pm 3.8 (0.66; 0.5)	24.0 \pm 6.4 (1.81; 1.1)	42.3 \pm 3.2 (3.19; 4.2)
$\Delta cobW3 \Delta cobW2::dis$	3.6 \pm 0.7 (0.18; 1.8)	16.1 \pm 2.4 (4.50; 4.0)	39.0 \pm 3.5 (10.9; 8.4)
$\Delta zupT$	7.3 \pm 1.5 (0.36; 1.3)	24.9 \pm 1.8 (3.42; 5.3)	63.4 \pm 1.4 (8.70; 19)
$\Delta zupT \Delta cobW3$	9.9 \pm 1.0 (1.35; 1.0)	30.0 \pm 2.8 (3.04; 5.3)	62.7 \pm 6.0 (6.36; 7.6)
$\Delta zupT \Delta cobW2::dis$	7.2 \pm 1.7 (0.99; 0.0)	25.5 \pm 0.7 (3.54; 7.6)	53.6 \pm 3.2 (7.43; 9.4)
$\Delta zupT \Delta cobW3 \Delta cobW2::dis$	7.9 \pm 0.7 (1.09; 0.3)	24.7 \pm 2.5 (3.11; 5.2)	60.9 \pm 4.0 (7.67; 11)
$\Delta dmeF$	20.8 \pm 6.6 (1.04; 0.0)	72.1 \pm 7.0 (3.47; 3.8)	129.7 \pm 13.7 (6.24; 5.4)
$\Delta dmeF \Delta cobW3$	5.1 \pm 0.7 (0.24; 2.2)	42.1 \pm 1.1 (8.29; 21)	119.0 \pm 10.7 (23.4; 10)
$\Delta dmeF \Delta cobW2::dis$	14.8 \pm 4.2 (0.71; 0.6)	62.6 \pm 2.8 (4.24; 6.8)	149.9 \pm 12.7 (10.2; 8.0)
$\Delta dmeF \Delta cobW3 \Delta cobW2::dis$	6.0 \pm 1.1 (0.29; 1.9)	45.3 \pm 1.8 (7.58; 14)	140.7 \pm 6.7 (23.5; 17)
$\Delta dmeF \Delta zupT$	16.4 \pm 1.9 (0.82; 0.3)	55.8 \pm 5.0 (3.40; 5.7)	n.d.
$\Delta dmeF \Delta zupT \Delta cobW3$	18.1 \pm 1.2 (1.10; 0.6)	55.5 \pm 3.3 (3.07; 8.5)	n.d.
$\Delta dmeF \Delta zupT \Delta cobW2::dis$	13.4 \pm 1.5 (0.82; 0.9)	55.1 \pm 8.6 (4.10; 4.1)	n.d.
$\Delta dmeF \Delta zupT \Delta cobW3$	12.8 \pm 2.4 (0.78; 0.8)	81.7 \pm 7.9 (6.36; 6.7)	n.d.
$\Delta cobW2::dis$			

^aThe cells were cultivated in standard TMM medium (160 nM Zn) with and without added Co(II). The metal content was measured using the ICP-MS, and the cobalt content of the cells in 1,000 Co per cell is shown. The experiment was repeated with three biological replicates, and standard deviations are indicated. The value is followed by a ratio D of the cobalt contents of the cells followed by a D value in parentheses. In cells cultivated without added cobalt, the Co contents of the $\Delta zupT$ and the $\Delta dmeF$ mutants were compared with the value for the parental strain, AE104. The content for the $\Delta cobW$ deletion mutants was compared with the value of the respective AE104, $\Delta zupT$, or $\Delta dmeF$ strains. For cells cultivated with added Co, the values were compared with that of the respective mutant strain grown without added Co. Given is the ratio Q and the D-value in parentheses. The full metal table is provided in the Supplement. Bold faced values indicate (0.66 < Q OR Q > 1.5) and (D > 1). Three biological repeats were performed; n.d., not done because of the high sensitivity of the respective strains.

either *cobW2*, *cobW3*, or both genes together (Table 3). All four $\Delta zupT$ strains had a higher Co ion content in this medium than the AE104 $\Delta cobW3$ mutant. When 1 μM or 5 μM Co(II) was added, all four $\Delta zupT$ mutants accumulated similar amounts of cobalt, which were always higher in the $\Delta zupT$ mutants than in the strains that had a native *zupT* gene.

Thus, CobW3 proved to be essential for the accumulation of cobalt in cells cultivated in standard TMM without added cobalt and depended on the presence of ZupT for accumulation of the cation. The lack of CobW3 caused a stronger decrease in cobalt import in the presence of ZupT than in its absence. CobW3 and ZupT may be involved in a downregulation of cobalt import by other import systems, for example, the CorAs, when sufficient zinc is available. Alternatively or additionally, CobW3 and ZupT together may stimulate efflux of Co under these conditions. CobW2 played a minor role in the control of cobalt accumulation in these cells.

CobW2 and CobW3 control the cellular flow-equilibrium of zinc in *C. metallidurans*

Zinc homeostasis in *C. metallidurans* is based on the control of a flow-equilibrium between uptake and efflux reactions, in addition to an effect caused by the metal-binding cytoplasmic components glutathione and polyphosphate (18). Pulse-chase experiments were performed to investigate how CobW2 or CobW3 affects this flow-equilibrium of zinc. Cells were cultivated in TMM adjusted to 200 nM Zn(II) (ambient Zn, aZn), low zinc (lZn), and metal-starvation medium (lZn_lMg), which is low zinc TMM with 100 μM instead of 1 mM Mg(II) (Table S1) to the exponential phase of growth. Harvest and washed cells were then loaded for 20 min with 1 μM radioactive ^{65}Zn and subsequently chased with 100 μM non-radioactive zinc. The cellular ^{65}Zn content of the cells was measured as described (18), with a control that was not chased. The results obtained for AE104 and $\Delta zupT$ results have already been published (18) but were obtained in the same experimental series as the data for the $\Delta cobW$ mutants, and these data are shown again for reference (Fig. 2; Fig. S2 to S4). From the pulse-chase results, the initial uptake rate of ^{65}Zn (v_{up}), the cellular zinc content after the uptake period C_{20} , the ratio of the extrapolated maximum zinc content of the uptake period C_{max} divided by C_{20} , the initial efflux rates v_{eff} of the chase period in the chased and non-chased control cells, and the ratio of the zinc contents at 40 min C_{40} divided by C_{20} were calculated (Table 4).

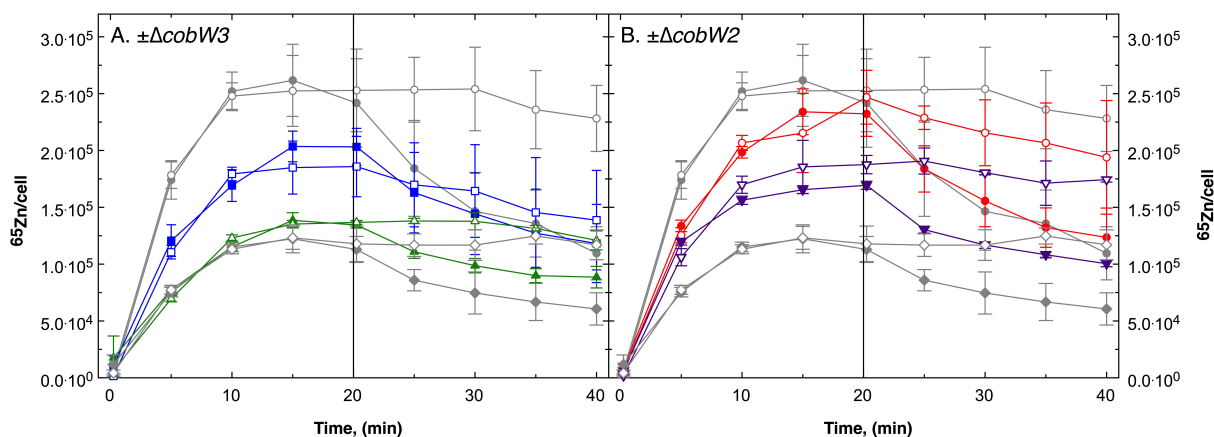


FIG 2 Pulse-chase experiment with *C. metallidurans* strains AE104, and its isogenic $\Delta cobW2$ and $\Delta cobW3$ mutants. Cells of strain AE104 (gray circles), $\Delta zupT$ (grey diamonds), $\Delta cobW3$ (blue squares), $\Delta cobW2$ (red circles), $\Delta zupT \Delta cobW2$ (purple inverted triangles), and $\Delta zupT \Delta cobW3$ (green triangles) were cultivated in low Zn and low Mg (0.1 mM Mg(II)) TMM. Panel A shows the strains without *cobW3*. Panel B those without *cobW2*. After cell-harvest, washing and suspension in uptake buffer, the cells were incubated in the presence of 1 μM ^{65}Zn (II) in the pulse phase and chased at $t = 20$ min with 100 μM non-radioactive Zn(II) (black symbols), or remained unchased (open symbols). The data for strains AE104 and $\Delta zupT$ have already been published (18) and were obtained in the same experimental series as the other data.

TABLE 4 Summary of the ⁶⁵Zn pulse-chase experiments

Medium	Uptake (pulse)			Chase		Pulse continued (control)	
	$v_{up} (s^{-1}), \% AE104$	$C_{20}, 1000 Zn/cell$	C_{max}/C_{20}	$v_{eff} (s^{-1}), \% AE104$	C_{40}/C_{20}	$v_{eff} (s^{-1}), \% AE104$	C_{40}/C_{20}
Ambient Zn							
AE104 ^a	162 ± 25; 100% ± 15%	96 ± 7; 100% ± 7%	2.20	112.3 ± 1.0; 100.0% ± 0.9%	37.2% ± 6.7%	-14.4 ± -0.2; -12.8% ± -0.2%	127.0% ± 8.8%
$\Delta zupT^a$	94 ± 7; 58% ± 4%	64 ± 4; 66% ± 4%	2.67	38.8 ± 0.3; 34.5% ± 0.2%	46.4% ± 12.7%	2.1 ± 0.0; 1.9% ± 0.0%	102.5% ± 2.5%
$\Delta cobW2$	111 ± 4; 69% ± 3%	73 ± 2; 75% ± 2%	2.43	32.2 ± 0.0; 28.6% ± 0.0%	57.2% ± 10.0%	9.3 ± 0.0; 8.3% ± 0.0%	86.3% ± 17.9%
$\Delta cobW3$	90 ± 1; 56% ± 0%	54 ± 5; 56% ± 5%	1.99	23.7 ± 0.2; 21.1% ± 0.2%	61.9% ± 11.0%	-4.8 ± 0.0; -4.3% ± 0.0%	120.3% ± 21.6%
$\Delta zupT \Delta cobW2$	96 ± 3; 59% ± 2%	83 ± 4; 87% ± 4%	4.66	15.5 ± 0.0; 13.8% ± 0.0%	82.2% ± 4.4%	-11.1 ± 0.0; -9.9% ± 0.0%	115.2% ± 8.4%
$\Delta zupT \Delta cobW3$	94 ± 4; 58% ± 2%	49 ± 8; 51% ± 8%	1.73	3.2 ± 0.0; 2.8% ± 0.0%	99.6% ± 37.6%	-4.0 ± 0.0; -3.6% ± 0.0%	99.9% ± 53.5%
Low zinc							
AE104 ^a	227 ± 17; 100% ± 8%	92 ± 3; 100% ± 3%	1.62	125.4 ± 1.3; 100.0% ± 1.0%	45.2% ± 16.6%	-11.2 ± -0.1; -8.9% ± -0.1%	128.1% ± 10.4%
$\Delta zupT^a$	67 ± 1; 30% ± 0%	63 ± 4; 68% ± 4%	7.44	15.4 ± 0.1; 12.2% ± 0.0%	67.7% ± 2.1%	-6.7 ± 0.0; -5.3% ± 0.0%	118.8% ± 12.9%
$\Delta cobW2$	194 ± 34; 86% ± 15%	114 ± 6; 123% ± 6%	1.77	37.6 ± 0.1; 30.0% ± 0.1%	60.2% ± 10.0%	-11.3 ± -0.1; -9.0% ± 0.0%	109.2% ± 23.1%
$\Delta cobW3$	113 ± 28; 50% ± 12%	66 ± 5; 72% ± 6%	2.42	24.1 ± 0.0; 19.2% ± 0.0%	71.0% ± 10.5%	-4.8 ± 0.0; -3.8% ± 0.0%	104.0% ± 52.5%
$\Delta zupT \Delta cobW2$	97 ± 2; 43% ± 1%	73 ± 4; 79% ± 4%	3.04	13.4 ± 0.0; 10.6% ± 0.0%	85.1% ± 12.3%	1.3 ± 0.0; 1.1% ± 0.0%	96.1% ± 25.3%
$\Delta zupT \Delta cobW3$	104 ± 13; 46% ± 6%	67 ± 5; 73% ± 6%	2.41	7.1 ± 0.1; 5.6% ± 0.1%	93.2% ± 11.7%	-13.3 ± -0.1; -10.6% ± 0.0%	134.3% ± 33.4%
Low Zn and Mg							
AE104 ^a	1147 ± 351; 100% ± 31%	272 ± 28; 100% ± 10%	1.45	314.4 ± 3.0; 100.0% ± 0.9%	40.2% ± 8.6%	27.1 ± 0.1; 8.6% ± 0.0%	83.8% ± 10.7%
$\Delta zupT^a$	509 ± 10; 44% ± 1%	115 ± 4; 42% ± 1%	1.38	53.3 ± 0.2; 16.9% ± 0.1%	52.5% ± 12.3%	-2.1 ± 0.0; -0.7% ± 0.0%	101.4% ± 11.4%
$\Delta cobW2$	695 ± 72; 61% ± 6%	240 ± 10; 88% ± 4%	1.49	119.0 ± 0.4; 37.9% ± 0.1%	51.6% ± 10.8%	48.2 ± 0.0; 15.3% ± 0.0%	81.0% ± 20.9%
$\Delta cobW3$	677 ± 45; 59% ± 4%	195 ± 12; 71% ± 5%	1.42	86.9 ± 0.3; 27.6% ± 0.1%	60.8% ± 17.7%	46.3 ± 0.1; 14.7% ± 0.0%	71.3% ± 22.5%
$\Delta zupT \Delta cobW2$	788 ± 291; 69% ± 25%	178 ± 13; 66% ± 5%	1.36	65.2 ± 0.3; 20.7% ± 0.1%	56.2% ± 1.5%	16.3 ± 0.0; 5.2% ± 0.0%	97.7% ± 1.2%
$\Delta zupT \Delta cobW3$	382 ± 64; 33% ± 6%	136 ± 2; 50% ± 1%	1.63	44.7 ± 0.2; 14.2% ± 0.1%	65.3% ± 7.0%	14.1 ± 0.0; 4.5% ± 0.0%	89.2% ± 6.1%

^aData obtained in the same experimental series and already published (18).

Fully zinc-replete cells of the $\Delta zupT$, $\Delta cobW2$, $\Delta cobW3$, $\Delta zupT \Delta cobW2$, and $\Delta zupT \Delta cobW3$ mutants cultivated in aZn-TMM showed insignificant differences between their respective pulse-chase curves (Fig. S2 and S3); however, all mutants accumulated a lower amount of ^{65}Zn than the parent AE104 during the uptake phase, that is, after 20 min (Table 4). Although the parent was fully zinc-saturated after 20 min with 96,000 ^{65}Zn imported, the respective value was only 75% for $\Delta cobW2$, 66% for ($\Delta zupT$), and 50% for ($\Delta cobW3$, $\Delta zupT \Delta cobW3$). The lower zinc contents of the mutant cells led to a decrease of the initial efflux rate in the subsequent chase period, even as low as only 2.8% of the parental value for the $\Delta zupT \Delta cobW3$ double null mutant.

Under zinc-starvation conditions (low zinc medium), the pulse-chase curves of the mutant cells were also not significantly different from each other but were different from those of the parent (Fig. S4). The $\Delta cobW2$ mutant was not different from AE104 with respect to the initial uptake velocity and ^{65}Zn content C_{20} after the pulse period. Also, the $\Delta zupT \Delta cobW2$ double mutant accumulated more zinc than the $\Delta zupT$ mutant and with a higher initial uptake rate (Table 4). Nevertheless, the initial net efflux rate v_{eff} decreased in all mutants, including the $\Delta cobW2$ strain, in comparison to AE104, and the rate in $\Delta zupT \Delta cobW3$ mutant was reduced to 5.6% of the parental value.

Following cultivation under metal-starvation (for Zn, Co, Mg) (IZn_IMg metal-starvation TMM), the parent reached a maximum zinc content after only 15 min during the uptake period and even the non-chased control exported ^{65}Zn after this period, whereas the $\Delta zupT$ mutant reached a level of zinc that was 60% lower, and the mutant continued to import zinc into un-chased control cells (Fig. 2; Table 4 (18)). Introduction of a $cobW3$ deletion into this strain had a stronger negative effect than introduction of a $\Delta cobW2$ mutation (Fig. 2). The pulse-chase curves of the $\Delta zupT \Delta cobW3$ double null mutant (Fig. 2A, green triangles) was similar to that of the $\Delta zupT$ single mutant, whereas that of the $\Delta cobW3$ mutant (Fig. 2A, blue squares) lay between the $\Delta zupT$ mutant and the parental strain. The curve of the $\Delta zupT \Delta cobW2$ double null mutant lay between that of the $\Delta zupT$ mutant and the parental strain and that of the $\Delta cobW2$ mutant lay between that of the $\Delta zupT \Delta cobW2$ double mutant and its parent (Fig. 2B). All mutants accumulated ^{65}Zn with a lower initial uptake rate than AE104 and accumulated lower amounts of zinc after 20 min, except for the $\Delta cobW2$ mutant (Table 4). All mutants also exported ^{65}Zn with a lower net efflux rate than the parent, with rates between 38% of the parental value in the $\Delta cobW2$ single mutant and as low as 14% in the $\Delta zupT \Delta cobW3$ double null mutant (Table 4).

ZupT, in cooperation with CobW2 and CobW3, influenced the flow-equilibrium of zinc. The effect of a lack of CobW2 was smaller compared with when the gene encoding CobW3 was deleted. In contrast, the effect on the flow-equilibrium was stronger in zinc-replete cells than in zinc- or metal-starved cells. Without these CobW proteins, the initial uptake rates, zinc contents after 20 min incubation with 1 μM Zn(II), and initial net efflux rates were lower compared with the parent. As indicated by the results from metal-starved cells, lack of CobW2 and CobW3 impacted zinc import by ZupT, as well as on other uptake systems (Fig. 2), with a $\Delta cobW2$ deletion even increasing zinc import in a $\Delta zupT$ background (Fig. 2B). Thus, these three proteins together seem to control zinc homeostasis in *C. metallidurans* (Table 4), and they also influence the cobalt content of the cells (Table 3).

ZupT, CobW2, and CobW3 control the cellular zinc pools

The pulse-chase experiments with radioactive ^{65}Zn were performed in parallel with experiments using isotope-enriched stable ^{67}Zn solutions (18). This allowed us to differentiate between a zinc pool, ZP1, containing zinc with the natural isotope composition and a ZP2 stemming from the isotope-enriched ^{67}Zn solution. The cells were cultivated in ambient zinc (aZn), zinc-starvation (IZn), and zinc-magnesium-, metal-starvation (IZn_IMg) medium with zinc in the natural isotope composition. Incubation was for 20 min with 1 μM ^{67}Zn (II) and chased for an additional 20 min with 100 μM zinc, again with the natural isotope composition. In this way, ZP2 represented the zinc imported

during the uptake phase, and ZP1 represented zinc that was initially present in the cells and also at the end of the experiment.

As with radioactive zinc, deletion of the genes for ZupT and both CobWs decreased the initial zinc content in ZP1 in zinc-replete cells (Table 5). The strongest effect was measured in the $\Delta zupT \Delta cobW3$ double null mutant. Incubation of cells with 1 μM ^{67}Zn resulted in zinc appearing in ZP2, a decrease of zinc in ZP1 but insignificant change in the overall zinc content, that is, ZP1 + ZP2. Zinc ions that were initially present in cells were exchanged against incoming zinc ions, and ZupT, CobW2, and CobW3 were not required for this turnover of zinc (Table 5). During the subsequent chase, zinc was mainly exported or exchanged from ZP2, despite the overall zinc content increasing in the cells. In zinc-replete cells, deletion of either of the three genes *zupT*, *cobW2*, or *cobW3* individually resulted in a decreased Co and Ni content of the cells (Table S5).

In low-zinc and in low-zinc, low-magnesium media, the cellular zinc content of the cells was lower compared with zinc-replete (aZn) cells, as expected. The high zinc content in the cells of the $\Delta zupT$ strain after growth in low-zinc medium was twice as high as in all other comparable experimental series and was not considered. Compared with zinc-replete cells, no zinc was exported from ZP1 during the uptake phase in zinc-starved cells, and more zinc remained in ZP2 during the subsequent chase. The exception was the parent in low-zinc, low-magnesium medium. This strain decreased the zinc content in ZP1 during the uptake phase, but its mutant derivatives did not. The zinc content in ZP2 was particularly low in cells of the zinc-starved $\Delta zupT \Delta cobW3$ double null mutant compared with the other cells, both before and after the chase (Table 5).

These results allow us to propose that the three proteins ZupT, CobW2, and CobW3 are required to adjust the cellular zinc pools under all conditions examined. The absence of ZupT and CobW3 results in decreased uptake of zinc, whereas efflux of zinc during the chase period was barely affected (Table 5, clearance of ZP2 during the chase period).

TABLE 5 Summary of the experiments with stable ^{67}Zn that accompanied the pulse-chase experiments with radioactive $^{65}\text{Zn}^b$

Strains	Initial 10^3 Zn			10^3 Zn after pulse			10^3 Zn after chase (0.1 mM)			
	Medium	ZP1	ZP2; %ZPt	ZP1 + ZP2	ZP1	ZP2; %ZPt	ZP1 + ZP2	ZP1	ZP2; %ZPt	ZP1 + ZP2
Ambient Zn										
AE104 ^a	103 ± 9	0.0 ± 0.2; 0.0%	103 ± 9	76.6 ± 1.8	27.4 ± 2.2; 26.4%	104 ± 4	240 ± 20	6.1 ± 0.8; 2.5%	246 ± 21	
$\Delta zupT^a$	42.8 ± 1.8	<0	42.6 ± 1.7	37.8 ± 2.1	20.5 ± 1.2; 35%	58.3 ± 3.3	226 ± 15	4.1 ± -0.1; 2%	230 ± 14	
$\Delta cobW2$	73.9 ± 2.6	<0	73.6 ± 2.6	60.9 ± 0.6	21.8 ± 1.3; 26%	82.8 ± 1.9	212 ± 26	3.7 ± 0.3; 2%	215 ± 26	
$\Delta cobW3$	77.1 ± 2.1	<0	76.8 ± 2.1	64.8 ± 1.6	21.9 ± 1.3; 25%	86.7 ± 2.9	307 ± 44	3.8 ± 0.2; 1%	311 ± 44	
$\Delta zupT \Delta cobW2$	57.8 ± 8.8	<0	57.6 ± 8.8	46.9 ± 6.5	20.8 ± 0.4; 31%	67.7 ± 6.9	238 ± 15	4.3 ± 0.1; 2%	243 ± 15	
$\Delta zupT \Delta cobW3$	40.3 ± 0.8	<0	40.2 ± 0.8	36.1 ± 1.1	15.1 ± 0.7; 29%	51.1 ± 1.8	168 ± 8	4.1 ± 0.0; 2%	172 ± 7	
Low Zn										
AE104 ^a	11.0 ± 1.9	0.0 ± 0.0; 0.1%	11.1 ± 1.9	6.7 ± 0.7	79.4 ± 5.3; 92.3%	86.1 ± 6.0	181 ± 17	24.6 ± 1.4; 12.0%	206 ± 19	
$\Delta zupT^a$	43.2 ± 1.4	<0	43.0 ± 1.4	37.0 ± 0.8	30.8 ± 2.5; 45%	67.8 ± 3.3	190 ± 8	6.9 ± 0.2; 4%	197 ± 8	
$\Delta cobW2$	8.9 ± 4.5	0.0 ± 0.0; 0%	8.9 ± 4.5	9.5 ± 3.9	58.4 ± 1.4; 86%	67.9 ± 5.3	180 ± 3	15.5 ± 0.8; 8%	196 ± 4	
$\Delta cobW3$	8.9 ± 4.6	0.0 ± 0.0; 0%	8.9 ± 4.5	15.4 ± 6.6	42.8 ± 1.7; 74%	58.2 ± 8.3	166 ± 9	15.1 ± 0.3; 8%	182 ± 10	
$\Delta zupT \Delta cobW2$	5.3 ± 0.5	0.0 ± 0.0; 1%	5.3 ± 0.5	8.3 ± 3.1	53.5 ± 0.7; 87%	61.8 ± 3.8	161 ± 3	14.1 ± 0.3; 8%	176 ± 4	
$\Delta zupT \Delta cobW3$	10.1 ± 6.4	0.0 ± -0.1; 0%	10.1 ± 6.3	8.3 ± 5.5	12.5 ± 0.2; 60%	20.7 ± 5.7	138 ± 13	4.7 ± -0.1; 3%	143 ± 13	
Low Zn and Mg										
AE104 ^a	29.5 ± 10.2	0.5 ± 0.0; 1.6%	30.0 ± 10.1	6.3 ± 1.3	85.0 ± 3.9; 93.1%	91.3 ± 5.3	201 ± 33	25.4 ± 2.0; 11.2%	226 ± 35	
$\Delta zupT^a$	8.3 ± 0.8	<0	8.3 ± 0.8	8.0 ± 0.3	57.4 ± 3.0; 88%	65.4 ± 3.3	169 ± 22	13.9 ± 0.3; 8%	183 ± 22	
$\Delta cobW2$	21.4 ± 10.4	<0	21.4 ± 10.3	20.0 ± 10.1	56.3 ± 9.0; 74%	76.3 ± 19.1	175 ± 14	14.6 ± 3.0; 8%	190 ± 17	
$\Delta cobW3$	11.9 ± 1.3	7.0 ± 9.4; 37%	18.9 ± 10.8	10.2 ± 1.2	40.4 ± 2.6; 80%	50.6 ± 3.8	166 ± 22	14.9 ± 0.1; 8%	181 ± 23	
$\Delta zupT \Delta cobW2$	12.9 ± 4.0	<0	12.9 ± 4.0	11.4 ± 3.0	57.6 ± 2.0; 83%	69.1 ± 5.0	174 ± 6	13.8 ± 0.8; 7%	188 ± 7	
$\Delta zupT \Delta cobW3$	10.4 ± 0.4	<0	10.4 ± 0.4	8.4 ± 0.5	14.2 ± 0.9; 63%	22.6 ± 1.4	171 ± 7	5.5 ± 0.0; 3%	177 ± 7	

^aData obtained in the same experimental series and already published (18).

^bThe cells of the indicated *C. metallidurans* mutants were incubated in Tris-buffered mineral salts medium adjusted to 200 nM Zn(II) (ambient zinc); the same medium without trace element solution SL6 and 0.1 mM Mg(II) instead of 1 mM Mg(II) (low Zinc and Mg), or TMM medium without SL6 but with 1 mM Mg(II) (low Zn). Zinc coming from SL6 or contaminations was in the natural isotope composition. These cells were incubated with 1 μM enriched stable ^{67}Zn for 20 min (pulse) and subsequently chased with 100 μM Zn(II) (or 1 mM when indicated) with the natural isotope composition. The zinc pools ZP1 and ZP2 were calculated from the ICP-MS measurements and ZPt = ZP1+ZP2 was determined.

ZupT, CobW2, and CobW3 affect Co, Cd, and EDTA resistance

Single or double deletions of *cobW2* and/or *cobW3* in the *C. metallidurans* parental strain AE104 did not decrease zinc or cobalt resistance, but cadmium resistance was decreased (Table 6). In the double mutant resistance to the metal cation-chelator, ethylenediaminetetraacetate (EDTA) was also decreased (Table 6). This decrease in resistance was even stronger in the $\Delta zupT$ background. Here, cobalt resistance was reduced to 43% in the $\Delta zupT$ mutant and 8% in the $\Delta zupT \Delta cobW3$ double null mutant, whereas a $\Delta cobW2$ deletion did not decrease any further the low cobalt resistance level of the $\Delta zupT$ mutant. The pattern of EDTA resistance in the $\Delta zupT$ mutant was similar to that for its cobalt resistance and accounted for a reduction in resistance to 45% in $\Delta zupT$ compared with the parent, and a further minor decrease in the $\Delta zupT \Delta cobW2$ double mutant, but resistance was decreased to 10% of the $\Delta zupT$ resistance level in the $\Delta zupT \Delta cobW3$ mutant (Table 6).

The effect of these gene deletions in reducing resistance was even stronger with respect to cadmium resistance, where a decrease down to 23% of the parental level in the $\Delta zupT$ mutant was observed. A further decrease to 23% compared with the level in the $\Delta zupT$ mutant was observed for the $\Delta zupT \Delta cobW2$ double mutant, and an even stronger decrease down to 12% was measured for the $\Delta zupT \Delta cobW3$ double mutant (Table 6). Additional deletion of *cobW2* increased the low cobalt and EDTA resistance level of the $\Delta zupT \Delta cobW3$ double mutant to approximately the level of the $\Delta zupT$ mutant. In contrast, cadmium resistance was not affected by the additional deletion of *cobW2* in the $\Delta zupT \Delta cobW3$ strain.

These data suggest that CobW2 and CobW3 cooperate to mediate full cadmium resistance in the parental strain and in its $\Delta zupT$ mutant derivative. On the other hand, the absence of CobW3 decreased cobalt and EDTA resistance in the $\Delta zupT$ strain, but not in the parent. This strong effect of a $\Delta cobW3$ deletion in the $\Delta zupT$ strain with respect to the Co and EDTA resistance, but not the Cd resistance, was reversed again by further deletion of *cobW2*, indicating that CobW2 mediated the low Co and EDTA resistance level in the $\Delta zupT \Delta cobW3$ double mutant.

DmeF is an important valve for the release of surplus cobalt ions

The three proteins ZupT, CobW2, and CobW3 control accumulation of cobalt in zinc-starved cells and are involved in resistance to Co, Cd, and EDTA. The main cadmium

TABLE 6 IC₅₀ values of mutant strains^a

Strain	Zn (μM)	Co (μM)	Cd (μM)	EDTA (μM)
AE104	114.2 ± 15.6 (1.00; 0.0)	193 ± 9 (1.00; 0.0)	174 ± 10 (1.00; 0.0)	1,652 ± 58 (1.00; 0.0)
$\Delta cobW3$	94.3 ± 2.8 (0.83; 1.1)	176 ± 14 (0.91; 0.7)	114 ± 15 (0.65; 2.4)	1,353 ± 180 (0.82; 1.3)
$\Delta cobW2::dis$	96.0 ± 7.4 (0.84; 0.8)	182 ± 15 (0.94; 0.5)	112 ± 5 (0.65; 4.1)	1,185 ± 156 (0.72; 2.2)
$\Delta cobW3 \Delta cobW2::dis$	92.4 ± 4.9 (0.81; 1.1)	174 ± 19 (0.90; 0.6)	87.5 ± 12.3 (0.50; 3.9)	975 ± 276 (0.59; 2.0)
$\Delta zupT$	86.8 ± 3.8 (0.76; 1.4)	83.8 ± 4.8 (0.43; 7.7)	39.1 ± 3.8 (0.23; 9.9)	739 ± 154 (0.45; 4.3)
$\Delta zupT \Delta cobW3$	65.0 ± 5.6 (0.75; 2.3)	6.6 ± 0.1 (0.08; 15.8)	4.8 ± 1.2 (0.12; 6.9)	75.5 ± 19 (0.10; 3.8)
$\Delta zupT \Delta cobW2::dis$	108.2 ± 1.2 (1.25; 4.3)	93.0 ± 9.0 (1.11; 0.7)	9.0 ± 0.2 (0.23; 7.5)	548 ± 96 (0.74; 0.8)
$\Delta zupT \Delta cobW3 \Delta cobW2::dis$	78.4 ± 1.7 (0.90; 1.5)	86.1 ± 3.4 (1.03; 0.3)	4.3 ± 0.0 (0.11; 9.2)	523 ± 230 (0.71; 0.6)
$\Delta dmeF$	106.6 ± 8.7 (0.93; 0.3)	5.5 ± 0.7 (0.03; 18.7)	149 ± 25 (0.86; 0.7)	1,343 ± 348 (0.81; 0.8)
$\Delta dmeF \Delta cobW3$	97.6 ± 2.0 (0.92; 0.8)	7.9 ± 0.6 (1.44; 1.8)	132 ± 17 (0.89; 0.4)	1,921 ± 222 (1.43; 1.0)
$\Delta dmeF \Delta cobW2::dis$	98.5 ± 2.1 (0.92; 0.8)	5.2 ± 0.4 (0.95; 0.3)	113 ± 6 (0.76; 1.1)	1,809 ± 164 (1.35; 0.9)
$\Delta dmeF \Delta cobW3 \Delta cobW2::dis$	97.6 ± 2.6 (0.92; 0.8)	6.2 ± 0.3 (1.13; 0.7)	104 ± 11 (0.70; 1.2)	1,721 ± 268 (1.28; 0.6)
$\Delta dmeF \Delta zupT$	78.0 ± 1.7 (0.68; 2.10)	2.1 ± 0.1 (0.01; 20.1)	40.5 ± 1.7 (0.23; 11.5)	1,263 ± 17 (0.76; 5.19)
$\Delta dmeF \Delta zupT \Delta cobW3$	77.0 ± 2.3 (0.99; 0.26)	2.6 ± 0.2 (1.22; 1.44)	72.9 ± 0.9 (1.80; 12.5)	1,578 ± 34 (1.25; 6.20)
$\Delta dmeF \Delta zupT \Delta cobW2::dis$	73.6 ± 3.4 (0.94; 0.87)	2.3 ± 0.1 (1.06; 0.47)	12.9 ± 2.2 (0.32; 7.05)	1,017 ± 39 (0.81; 4.45)
$\Delta dmeF \Delta zupT \Delta cobW3 \Delta cobW2::dis$	75.5 ± 1.4 (0.97; 0.81)	2.5 ± 0.0 (1.18; 1.96)	13.8 ± 4.5 (0.34; 4.30)	686 ± 93 (0.54; 5.28)

^aStandard TMM. Bold-faced if [(Q > 1.5 OR Q < 0.67) AND D > 1], meaning the ratios of two values are larger than 1.5 and the deviation bars do not overlap. Comparison of the $\Delta dmeF$ and the $\Delta zupT$ mutants to AE104 and of the $\Delta cobW$ mutants to their respective parent.

exporters in *C. metallidurans* are the P_{1B2}-type ATPases ZntA and CadA (15), whereas the CDF protein DmeF is required for cobalt export (15, 16). A $\Delta dmeF$ mutant showed impaired growth in the presence of 5 μM Co(II) in mZn medium (Fig. 3). The IC₅₀ of the mutant was 5.5 μM Co(II) compared with 193 μM in the parental strain, AE104 (Table 6). Resistance to zinc, cadmium, and EDTA was not influenced in the mutant. The CDF protein FieF in AE104 is required for resistance to iron (16, 45). Growth of a $\Delta fieF$ mutant was only slightly impaired compared with AE104, whereas a $\Delta dmeF \Delta fieF$ double mutant had a growth phenotype similar to the $\Delta dmeF$ single mutant (Fig. 3B). Additional deletion of the genes *cobW2*, *cobW3*, or both in the $\Delta dmeF$ strain had limited influence on resistance to Zn, Co, Cd, or EDTA (Table 6).

The cobalt content of cells of the $\Delta dmeF$ mutant cultivated in standard zinc medium was identical to that of the parent, AE104 (Table 3). When 1 μM or 5 μM Co was added, the level of the cation increased 3.5-fold and 6.2-fold, respectively, to a final level of 130,000 Co per cell, whereas the zinc content of the cells was not influenced (Table S4). These data confirm that DmeF is the major cobalt efflux system of *C. metallidurans* AE104. The CobWs did not mediate any level of cobalt resistance in the absence of DmeF (Table 6).

DmeF supports the function of the ZupT, CobW2, and CobW3 network

All mutants up to the quadruple mutant $\Delta dmeF \Delta zupT \Delta cobW3 \Delta cobW2::dis$ were constructed and characterized. Cobalt resistance of the $\Delta zupT$ mutant was 43% of the level of the parental strain, AE104, and that of the $\Delta dmeF$ mutant only 3% of the parent (Table 6). The IC₅₀ for Co(II) decreased to 1% of the parental level in the $\Delta dmeF \Delta zupT$ double deletion mutant (Table 6). In the presence of 1 μM Co(II), the double mutant grew more slowly than AE104, whereas both single mutants had similar growth rates that ranged between that of the double mutant and that of AE104 (Fig. 4A). In the absence of added Co(II), the $\Delta dmeF$ mutant grew like its parent, the $\Delta zupT$ mutant grew more slowly,

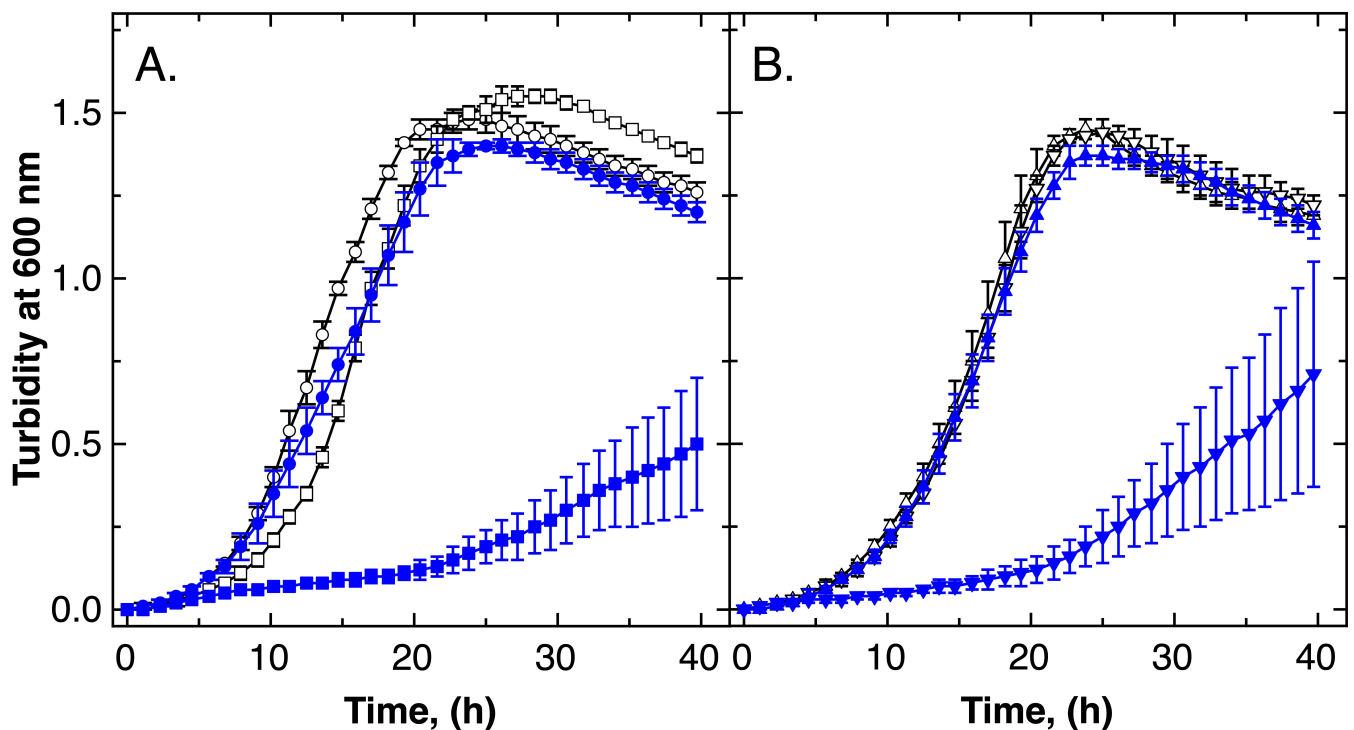


FIG 3 DmeF mediates cobalt resistance in *C. metallidurans*. Panel A shows time-dependent growth of the parental strain, AE104 (circles), and an isogenic $\Delta dmeF$ mutant (squares). Panel B shows data for a $\Delta fieF$ (triangles) mutant and a $\Delta dmeF \Delta fieF$ (inverted triangles) cultivated with (blue closed symbols) or without (black open symbols) 5 μM Co(II) in standard TMM. Data for three biological repeats with standard deviations are shown.

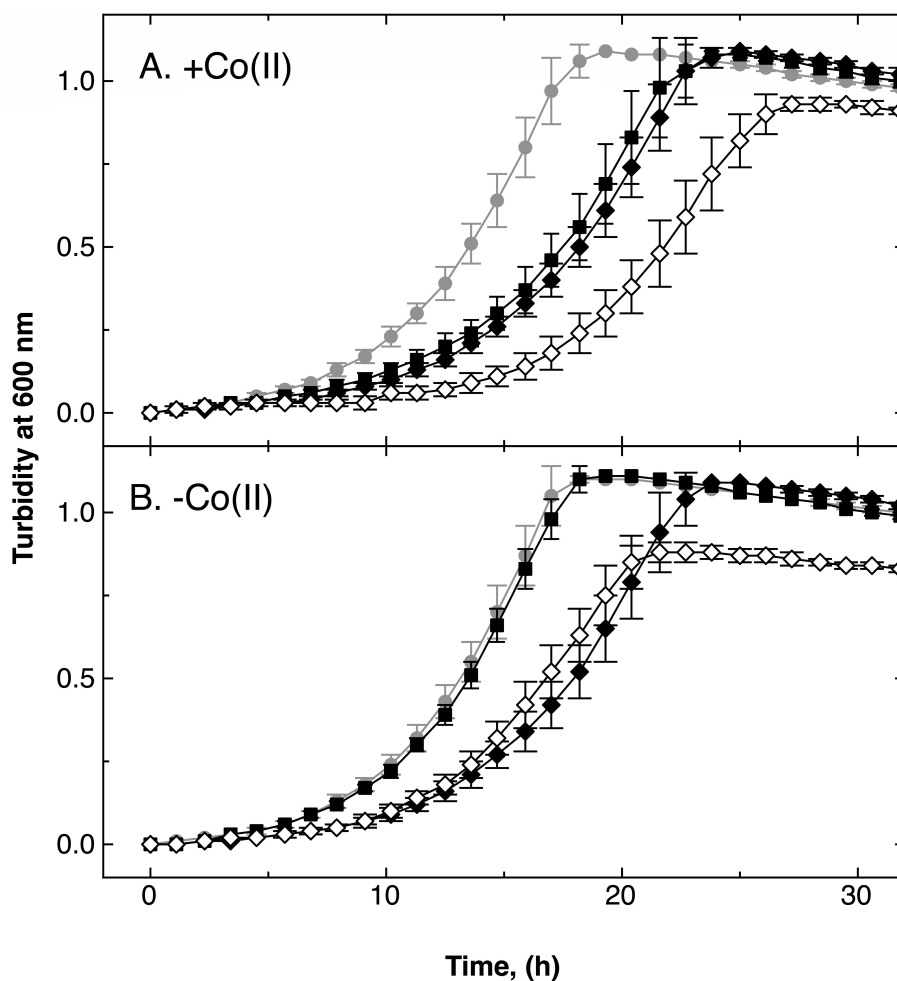


FIG 4 Effect of Co(II) on a $\Delta dmeF \Delta zupT$ double null mutant. Time-dependent growth curves of strains $\Delta zupT$ (closed diamonds), $\Delta dmeF$ (squares), and $\Delta dmeF \Delta zupT$ (open diamonds) in standard TMM medium without (panel B) or with (panel A) addition of 1 μM Co(II) are shown. Growth of the parental strain AE104 (closed circles) is shown in gray for reference. Data for three biological repeats with standard deviations were shown.

and the double mutant's growth rate was similar to that of the $\Delta zupT$ mutant, albeit with a lower growth yield (Fig. 4B). Both transport systems, the ZupT uptake, and the DmeF efflux systems, thus appear to cooperate to mediate cobalt resistance and also to allow the maximum growth yield in the absence of added Co(II) to be attained.

Deletion of *cobW2* or *cobW3* in the $\Delta dmeF$ isogenic strain increased Co resistance in the case of the $\Delta dmeF \Delta cobW3$ strain. The IC_{50} of the $\Delta dmeF \Delta cobW2$ strain did not change, however, and the triple mutant exhibited an IC_{50} like that of the $\Delta dmeF$ strain (Table 6). This effect was more clearly visible in growth curves done in the presence of 2.5 μM Co(II) (Fig. 5). The $\Delta cobW3$ deletion (Fig. 5, blue triangles) almost restored growth to the parental level, whereas the $\Delta cobW2$ deletion was less efficient in counteracting the growth delay mediated by the $\Delta dmeF$ mutation (green inverted triangles). The triple mutant had a growth rate that was between those of the $\Delta dmeF \Delta cobW2$ and $\Delta dmeF \Delta cobW3$ (magenta diamonds) mutants. This influence on the growth rate was only visible in the $\Delta dmeF$ mutant background and only in the presence of Co(II) (Fig. S5). Zinc, cadmium, and EDTA resistances were unchanged (Table 6). This suggests that CobW2 and CobW3 were responsible for the growth defect of the $\Delta dmeF$ mutant in the presence of Co(II). Moreover, both CobW proteins interacted with each other, with loss of CobW3 causing a more severe growth deficiency compared with loss of CobW2.

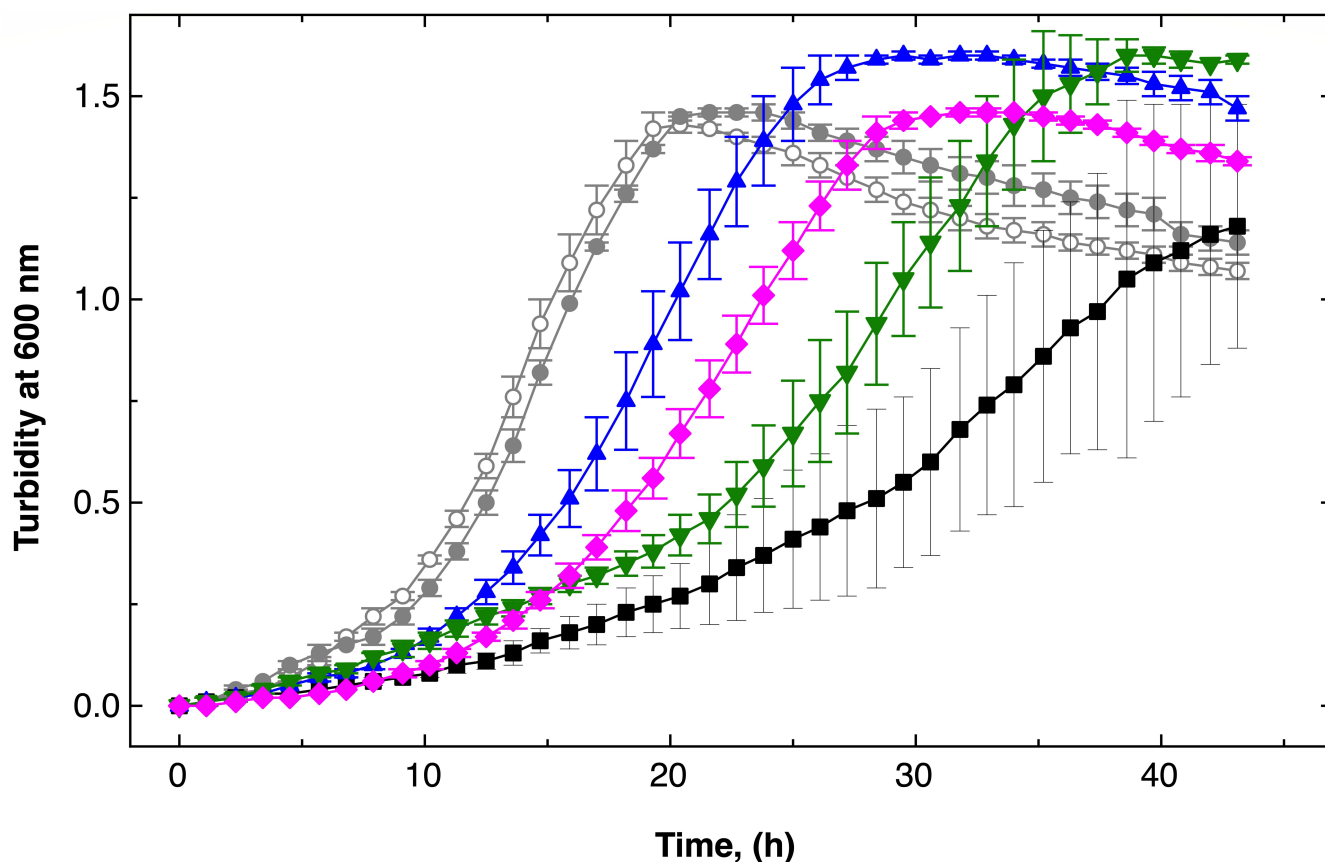


FIG 5 Strains lacking CobW2 and CobW3 show impaired growth in a $\Delta dmeF$ mutant background. Time-dependent growth of strains $\Delta dmeF$ (black filled squares), $\Delta dmeF \Delta cobW3$ (blue triangles), $\Delta dmeF \Delta cobW2::dis$ (green inverted triangles), and the $\Delta dmeF \Delta cobW3 \Delta cobW2::dis$ triple mutant (magenta diamonds) in standard TMM in the presence of 2.5 μM Co(II). Growth of the parental strain AE104 with (closed circles) and without (open circles) 2.5 μM Co(II) is shown in gray for reference. Three biological repeats were performed, and standard deviations are shown. Data for all strains and conditions tested are shown in Supplementary information.

Introduction of a deletion in either the *cobW2* or *cobW3* genes in the $\Delta dmeF \Delta zupT$ double mutant background also negatively affected growth in the presence or absence of 1 μM Co(II) (Fig. 6). In the presence of Co(II), the half-logarithmic plot shows that all growth curves were parallel with each other, except that of the parent, AE104 (Fig. S6). Compared with the parent in the presence of Co(II), the deletions affected the length of the lag-phase and the growth rate. Comparing the mutants with each other in the presence of Co(II) and in all comparisons in the absence of Co(II), only the length of the lag-phase was influenced.

When Co(II) was added, $\Delta dmeF$, $\Delta zupT$, and $\Delta dmeF \Delta zupT \Delta cobW3$ had the same growth delay, which was largest in the $\Delta dmeF \Delta zupT$ double mutant and between those of the quadruple mutant and the $\Delta dmeF \Delta zupT \Delta cobW2$ triple mutant (Fig. 6; Fig. S6). As in the $\Delta dmeF$ mutant, the CobWs were also responsible for the growth delay of the $\Delta dmeF \Delta zupT$ double mutant, but the difference in comparison to the $\Delta dmeF$ single mutant was that CobW2 no longer had any effect. In the absence of added Co(II), $\Delta dmeF$ mutant grew like the parent AE104, whereas most other mutants had growth phenotypes like the $\Delta zupT$ mutant, and only the $\Delta dmeF \Delta zupT \Delta cobW3$ strain had a growth phenotype between that of the $\Delta zupT$ and AE104. A decreased growth yield was only visible in the $\Delta dmeF \Delta zupT$ double mutant, and therefore, this was also due to CobW2 or CobW3 (Fig. 6).

Introduction of a $\Delta cobW3$ mutation into the $\Delta dmeF \Delta zupT$ double mutant increased Co resistance slightly, which was reminiscent of the phenotype of the $\Delta dmeF$ mutant;

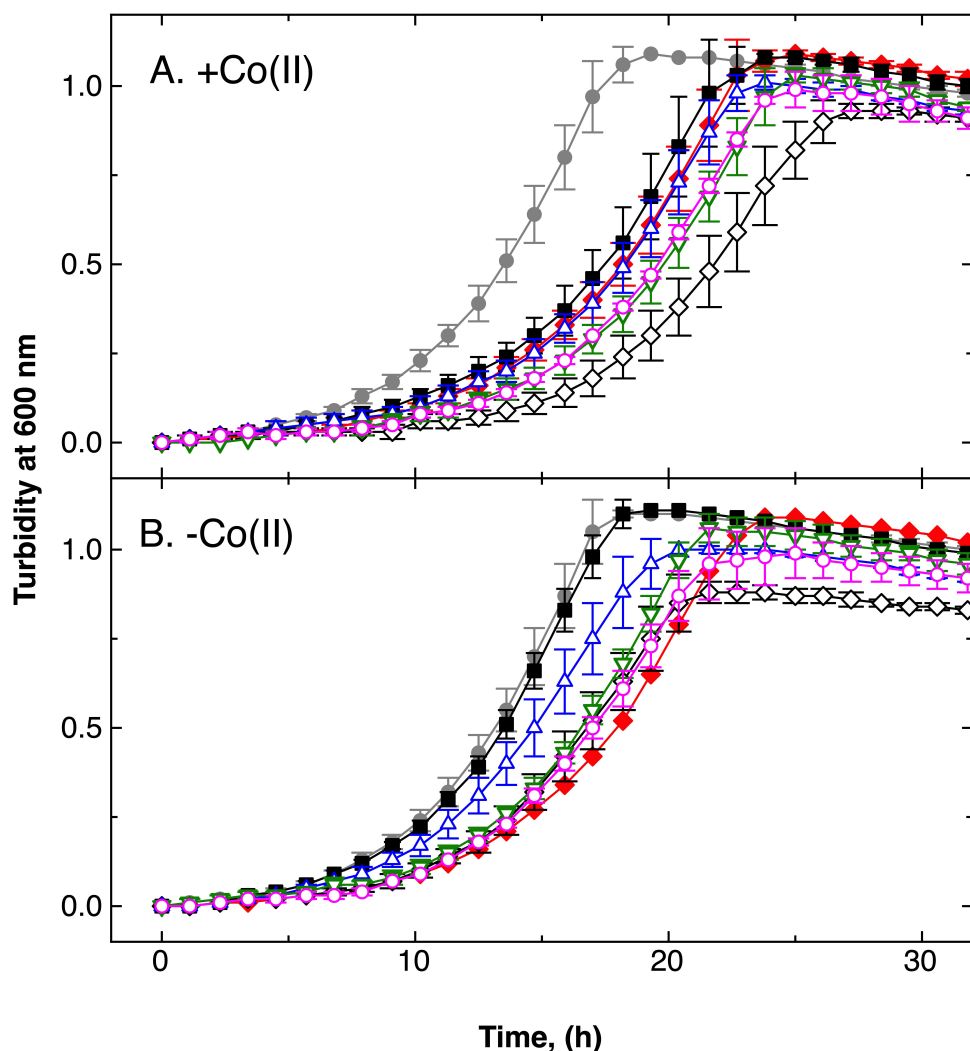


FIG 6 Effect of Co(II) on derivatives of the double deletion strain $\Delta zupT \Delta dmeF$. Time-dependent growth of strains $\Delta zupT$ (red filled diamonds), $\Delta dmeF$ (filled squares), $\Delta dmeF \Delta zupT$ (open diamonds), $\Delta dmeF \Delta zupT \Delta cobW2$ (green open inverted triangles), $\Delta dmeF \Delta zupT \Delta cobW3$ (blue open triangles), and $\Delta dmeF \Delta zupT \Delta cobW2 \Delta cobW3$ (magenta open circles) in standard TMM medium without (panel B) or with (panel A) 1 μM co(II). Growth of the parent AE104 (closed circles) and is shown in gray for references. Three repeats, deviations indicated.

introducing the $\Delta cobW2$ allele had no effect (Table 6). Although the $\Delta zupT$ deletion decreased the cobalt content in standard TMM down to 36% of the parent level, deletion of $zupT$ in the $\Delta dmeF$ mutant barely affected Co levels when compared with those of AE104 (Table 3). DmeF is therefore responsible for maintaining the low cobalt level in the $\Delta zupT$ strain. Moreover, although deletion of $cobW3$ had only a small effect in the $\Delta zupT$ background, the mutation strongly decreased the cobalt content in the parental strain and its isogenic $\Delta dmeF$ mutant. However, the $cobW3$ mutation had no effect in the $\Delta dmeF \Delta zupT$ double null mutant background. Thus, ZupT was responsible for maintaining the low cobalt levels of the parental strain and in a $\Delta dmeF$ mutant. This means that DmeF, ZupT, and CobW3 cooperate to adjust the cobalt content of the cells in standard TMM.

These effects of the DmeF, ZupT, and CobW3 network on the cobalt level were similar in cells grown in the standard TMM with or without 1 μM Co(II) (Table 3), but the cobalt level increased strongly in the $\Delta zupT \Delta dmeF \Delta cobW2 \Delta cobW3$ quadruple mutant in the presence of 1 μM Co(II). Cobalt resistance of the quadruple mutant was about

2 μM (Table 6) and did not change when CobW2 or CobW3 were present. Neither CobW mediated some degree of cobalt resistance in the absence of ZupT and DmeF. In the presence of DmeF and the $\Delta\text{zupT } \Delta\text{cobW2 } \Delta\text{cobW3}$ triple mutant, cobalt resistance increased 3-fold to about 6 μM (Table 6), so that ZupT caused a low degree of cobalt resistance, probably by mediating controlled uptake of Co(II). Again, presence of the CobWs in the ΔdmeF mutant background did not increase cobalt resistance, showing the importance of DmeF as central inner membrane efflux system for Co(II). Interestingly, cobalt resistance of the $\Delta\text{zupT } \Delta\text{cobW3}$ double mutant was at the level of that of the ΔdmeF mutants and increased again, when *cobW2* was additionally deleted (Table 6). This indicated that CobW2 also has a function in cobalt homeostasis, which may be based on some interplay with the efflux system DmeF.

Although the EDTA resistance was strongly reduced in the ΔzupT mutant and even more so in the $\Delta\text{zupT } \Delta\text{cobW3}$ double mutant, it was hardly changed in the ΔdmeF single mutant but was decreased in the $\Delta\text{dmeF } \Delta\text{zupT}$ mutant down to 76% of the parental level. It increased again marginally (1.25-fold) when the *cobW3* gene was additionally deleted and was decreased to 81% of the $\Delta\text{dmeF } \Delta\text{zupT}$ level by introduction of a ΔcobW2 allele and was reduced further to 54% in the $\Delta\text{cobW3 } \Delta\text{cobW2}$ mutant. CobW2 and CobW3 synergistically increased EDTA resistance in the presence of ZupT and DmeF, had no effect when DmeF was absent from cells but ZupT was present, and acted antagonistically when either transport system was absent; CobW2 increased and CobW3 decreased resistance. The strongest effect on EDTA resistance was observed in the absence of ZupT but in the presence of DmeF with CobW3 increasing EDTA resistance 10-fold in a CobW2-dependent manner. This indicates that this CobW2-dependent decrease in EDTA resistance in the $\Delta\text{zupT } \Delta\text{cobW3}$ mutant was also DmeF-dependent.

Although both CobWs contributed synergistically to Cd resistance in the presence of both transport systems, they had no effect in the ΔdmeF mutant. Deletion of ΔcobW3 increased Cd resistance nearly 2-fold in the $\Delta\text{dmeF } \Delta\text{zupT}$ double mutant while the same deletion decreased Cd resistance strongly in the ΔzupT strain. This effect was again CobW2-dependent. The IC_{50} for cadmium was similar in the quadruple mutant, the $\Delta\text{dmeF } \Delta\text{zupT } \Delta\text{cobW2}$ triple mutant, and the $\Delta\text{zupT } \Delta\text{cobW2}$ double mutant but was 2-fold higher than in the $\Delta\text{zupT } \Delta\text{cobW3 } \Delta\text{cobW2}$ triple and the $\Delta\text{zupT } \Delta\text{cobW3}$ double mutants. DmeF was thus responsible for the strong decrease in cadmium resistance in the $\Delta\text{zupT } \Delta\text{cobW3}$ double mutant (Table 6). This indicated that the ability to adjust the zinc and cobalt content through an interaction between ZupT, CobW2, CobW3, and DmeF is a prerequisite for the bacterium to adapt to metal starvation conditions and also for cadmium resistance. Zinc and cobalt homeostasis and cadmium resistance are linked processes in this bacterium with ZupT, CobW2, CobW3, and DmeF being the main actors in this multiple-ion homeostasis (Fig. S1).

DISCUSSION

The interplay between ZupT, CobW2, CobW3, and DmeF

A complicated interplay between ZupT with CobW2 and CobW3 (Fig. S1) affects the flow-equilibrium of Zn(II) in *C. metallidurans*, along with uptake of other metals, metal efflux systems, and the metal-binding components of the cytoplasm glutathione and polyphosphate (18). This maintains the number of Zn ions per cell at about 70,000 to 80,000 per cell, as previously published (8, 43). To accumulate this number of Zn ions per cell, a zinc content of the growth medium of 140 nM to 160 nM is needed, and indeed, at lower concentrations, all available Zn is accumulated by the cells (Table 2).

If the zinc content of the growth medium does not allow accumulation of 80,000 Zn ions per cell, *C. metallidurans* accumulates Co(II) (Fig. 1). This may allow us to metalate metal-promiscuous enzymes such as FoIE_IB1 and FoIE_IB2 to substitute Zn-dependent paralogs (25). ZupT and CobW3 are central to this process (Fig. 1; Tables 2 and 3), whereas CobW2 also contributes but in a minor way. The interplay of these three proteins is necessary for *C. metallidurans* to survive metal-starvation conditions, but it also contributes to cadmium and cobalt resistance (Table 3), with the Co efflux system

DmeF (16) also required for full resistance to both metals. DmeF is as important for full cobalt resistance as ZupT (Fig. 4). CobW2 and CobW3 cause delayed growth in a $\Delta dmeF$ mutant in the presence of ZupT, so that all four proteins are necessary not only to mediate cobalt resistance but also to allow cobalt accumulation in response to zinc starvation.

Cd(II) interacts with all thiol compounds in the cytoplasm, which leads to protein denaturation, limiting levels of glutathione, release of iron from enzymes such as aconitase and subsequently to redox stress (46–49). The influence of ZupT, DmeF, and the CobW proteins in cadmium resistance (Table 6) also indicates that cadmium may disturb zinc homeostasis. Both metals belong to the same group of the periodic system of the elements and are thus chemically related. Disturbance of zinc homeostasis by cadmium has been noted before (50, 51). This would indicate that a primary function of ZupT, DmeF, and the two CobWs would be to protect zinc homeostasis against cadmium by filling-up the zinc pool with available zinc. Under zinc-replete conditions, cadmium cannot outcompete Zn(II) because Cd(II) is a soft metal ion that prefers Cys over His residues, and both metal ions have different ionic radii (52, 53). Only if insufficient Zn(II) is available to fill-up the zinc pool is Cd(II) able to outcompete Zn(II) (40). Filling up the zinc pool with cobalt instead may thus help prevent this toxic effect of Cd(II).

This could be one important reason to fill-up parts of the cellular zinc pool with Co(II) in the event of zinc-limitation. Moreover, metal-promiscuous paralogs of zinc-dependent proteins could be supplied with cobalt to retain functionality (25). This would also explain the role of cobalt in zinc-starved *S. typhimurium* (38) and the link between Zn and Co homeostasis and Cd resistance in *C. metallidurans*. One of the functions of the CzcCBA transenvelope system, but which is absent in the AE104 strain, could be to prevent import of too much of either metal into the plasmid-bearing *C. metallidurans* CH34 cells. Because ZupT is required for the Zn-Co-Cd connection, this would explain why the CzcCBA efflux complex cannot exist in the absence of ZupT (43).

Binding of metals to the CobWs

The homologs of the CobWs are associated with the delivery of Zn(II) to Zn-dependent proteins in bacteria and eukaryotes (22, 23, 54, 55). Metal delivery is aided by GTP- or ZTP-hydrolysis (27) in the case of the CobW-ortholog ZagA. CobW1, which is only needed under extreme zinc-starvation conditions in *C. metallidurans* (20), is related to ZagA, ZNG1 from *Saccharomyces cerevisiae*, and CobW from *Rhodobacter capsulatus* (Fig. S7). All these proteins display the typical Walker A-, B-, switch-, and G-binding motifs of GTPases. The only difference between the GTPases and the ZTPase ZagA could be the Cys residue upstream of the highly conserved Asp residue in the G-binding motif (Fig. S1 and S7). With the exception of CobW3, all of these proteins have an internal metal-binding site between the Walker B and the switch motifs, which is highly conserved (GCI/mCC), strongly selective for soft and borderline transition metal cations, and is probably involved in triggering the GTPase activity (56). More importantly, binding of MgGTP pre-conditions this site for acceptance of the correct metal ions (41). Always in dependence of the extant cytoplasmic metal ion concentration, this, nevertheless, assures the correct metalation of a CobW homolog (40), so that CobW_Rcap from *R. capsulatus* accepts Co(II) but YeiR and YjiA accept Zn(II) (41), delivering it to the internal metal-binding site. This metal preference, modeled under *in vivo* conditions, however, was mirrored to some degree by the relationship between the respective proteins (Fig. S7). CobW_Rcap and YeiR form one deeply branched relationship; ZagA, CobW1, and CobW3 a second; YjiA, CobW2, and ZNG1 the third, which is again deeply branched.

In addition to the missing internal metal binding motif in CobW3, this protein and CobW2 contain large His-rich regions, which AlphaFold2 predicts to form a random coil (Fig. S1 and S7). This region is located at the C-terminus of CobW3 but is internal in CobW2. These motifs could indeed be intrinsically disordered protein (IDP) regions, which organize themselves during binding of metal cations. In this scenario, binding of one metal cation to CobW2 would be to the internal metal-binding site and controlled

by the *in vivo* concentration of a metal cation among those of competing metal cations. With increasing Co and decreasing Zn concentrations, the probability of Co-binding over Zn-binding would consequently increase.

Binding of metal cations to the putative IDP regions would not be controlled directly by MgGTP (41) but by the proportion of a metal among the other cations present in the cell. CobW3 binds about 8 (6.5 to 9) Zn(II) ions with decreasing affinity when only Zn(II) is present. When incubated with a metal mix, 4 Zn(II), 2 to 3 Ni(II), 1 Co(II), and 1 Cd(II) are bound (20). CobW2, with its large internal His-rich region, is present in two different conformations, binding 0.5 Zn(II) or about 7 Zn(II), respectively, when only zinc is present. When offered a mixture of metal cations, CobW2 precipitates (20). This led to the assumption that CobW2 is a zinc-storage protein that binds up to 7 Zn(II) ions in its "open" conformation and one or none Zn ions in its "closed" conformation. CobW2 could therefore act as a zinc buffer but, as shown by the CobW2-dependent decrease of Co resistance of the $\Delta zupT \Delta cobW3$ mutant (Table 6), may also interact in some way with DmeF. With about 2,000 copies per cell and 7 Zn(II) ions bound per protein, CobW2 would be able to store 14,000 Zn(II) of the total 70,000 Zn(II) ions in the cell (17, 20), representing 20% of the cellular zinc. CobW3, on the other hand, has a clear influence on metal import (20), and this is further substantiated by the findings of the current study. CobW3 may be capable of determining the relative proportions of metal cations in the metal mix through differential affinities by binding them at its C-terminal His-rich region. This would consequently affect metal transport depending on the actual metal cations bound.

Zinc homeostasis in *C. metallidurans*

As far as is known, zinc is an essential element for all organisms (23, 57). The divalent Zn(II) transition metal cation has a completely filled $3d^{10}$ orbital, which prevents the formation of stable octahedral complexes because no empty 3d orbitals are available to accept free electron pairs from metal ligands (58). Thus, Zn(II) forms tetrahedral complexes. These complexes have the function of stabilizing the conformation of proteins such as in the periplasmic Cu-Zn-dependent superoxide dismutase or in the RpoC (beta-prime) subunit of the RNA polymerase (59, 60). Alternatively, Zn(II) can also act as Lewis acid catalyzing biochemical reactions such as in alcohol dehydrogenase, carbonic anhydrase, or FoIE_{1A}-type GTP-cyclohydrolase I, which initiates biosynthesis of the essential cofactor tetrahydrofolate (25, 61).

As *C. metallidurans* typically contains 70,000 to 80,000 Zn(II) per cell when cultivated in standard TMM (8, 17, 43), high external zinc concentrations cause transient accumulation of zinc resulting in the cation being exported by the P_{IB2}-type ATPase ZntA in the plasmid-free strain AE104, whereas in the CH34 wild-type strain additional plasmid-encoded zinc efflux pumps eject excess zinc ions. Strain AE104 contains a much higher number of zinc-binding proteins, about 110,000 per cell (17), so that after growth in standard TMM, not all zinc-binding sites are occupied. Half of the zinc-binding proteins are involved in genetic information-processing, with two-thirds of these being zinc-binding ribosomal proteins and the remaining one third being zinc-binding proteins of the RNA polymerase. However, only about $4,709 \pm 128$ copies of RpoC per cell (17) need a zinc ion for correct folding, which is "checked" by the omega subunit RpoZ before final assembly of the RNAP. The lowest cellular zinc content measured in this study was $7,100 \pm 1,200$ Zn ions per cell (Table 1) in low zinc medium, which would leave about 2,400 Zn for other essential zinc-dependent proteins, for instance, the periplasmic SodC, with 164 ± 43 copies per cell (17).

An operon in *C. metallidurans* contains two Zur-binding sites at the promoter, is only expressed under extreme zinc starvation, and includes a gene encoding the third COG0523-family protein CobW1. The operon also has genes encoding a metal-promiscuous GTP-cyclohydrolase FoIE_{1B2} that needs Fe, Mn, or Co for activity, and paralogs of the zinc-dependent proteins CysS, QueD, AIIb, as well as a carbonic anhydrase (19, 20). The number of the respective paralogs total about 3,700 proteins (17), so that the 7,100

Zn ions per cell might indeed signify the lowest possible zinc content of these cells. As in case of the zinc-dependent GTP cyclohydrolase FoIE_{1A} and its metal-promiscuous substitutes FoIE_{1B1} and FoIE_{1B2} (28, 61, 62), other metal cations might act as Lewis acids in an essential biochemical catalysis, substituting for the lack of zinc.

As a consequence of the Debye-Hückel rule (63) and other constraints, Mg(II) and the divalent transition metal cations should form solvent-shared ions-pairs with the Lewis bases inside the cell and form contact ion-pairs whenever a sufficient number and position of Lewis base ligands are available (53). In contrast, the alkali metal cations Na(I) and K(I) should be mostly fully solvated ions, which counteract the negative charges of the proteins and nucleic acids, but otherwise can enter into solvent-shared ions-pairs with these compounds. The proteome of *C. metallidurans* may have a capacity of nearly 6 million binding sites for divalent metal cations, including those in the 110,000 proteins of the zinc repository (17, 53), which might interact with half of the 10 million Mg(II) ions per cell, if Mg(II) is not out-competed by transition metal cations. Moving from protein to protein, Zn(II) might follow the amino acids on their path to the translating ribosome. The ribosomal proteins and the RNA polymerase contain zinc buffers, with RNAP having additional zinc-binding sites besides the essential one in RpoC (17). In this way, Zn(II) is available to be inserted into nascent proteins during translation, which explains the zinc-dependence of translation (64). Proteins such as ZagA might be required for those proteins that did not, or could not, obtain their zinc during translation, or which have lost it.

Should this hypothetical zinc allocation pipeline become limiting for the cation, other metal cations may outcompete the Mg(II) and follow the amino acids to the ribosome. Cd(II), which belongs to the same group of the periodic system as Zn(II) and also has a completely filled d-orbital, may bind to zinc-binding sites in the absence of competing zinc ions, which explains the observed greater cadmium sensitivity of zinc-starved cells. Should Fe(II) enter this allocation pipeline, zinc-dependent proteins would receive the highly redox-active iron. This situation should be prevented by iron-storage proteins or by its rapid sequestration by Fe-dependent proteins, for example, in the form of Fe-S-clusters (30, 65). *C. metallidurans* does not use Mn(II) and handles Cu(I) by a sophisticated periplasmic copper homeostasis and export from the cytoplasm (8, 66). This leaves Co(II) and Ni(II) as the only other possible metal cations that may follow the zinc allocation pathway.

Cobalt and nickel

Ni(II) ions have eight electrons in their 3d orbital (58). An octahedral complex would have six electrons in the non-binding and the remaining two electrons in an anti-bonding 3d orbital, so that four ligands are firmly bound and the axial two are only loosely bound. Such Ni(II) complexes appear as square-planar complexes (41). The CnrCBA transenvelope efflux complex is responsible for nickel resistance in *C. metallidurans* (67). It is regulated by the extracytoplasmic sigma factor CnrH, bound in the absence of nickel by the membrane-bound CnrYX complex with CnrX being the sensor for periplasmic Ni(II) (68–70). CnrX binds Ni(II) in a quasi-octahedral complex (71–74). Two adjacent corners of the Ni(II) complex are occupied by the terminal carboxyl group of a glutamate residue. One anti-bonding d-orbital of the central Ni(II) ion contains the two electrons as an electron pair. This allows Ni(II) to accept one more electron pair from the deprotonated carboxyl group of the Glu ligand. The required pairing energy of the electrons is compensated by the release of energy stemming from the mesomeric overlay of one oxygen donating an electron pair to the Ni(II) as fifth ligand and the other double-bonded oxygen is not bonded by Ni(II) (74). This discriminates strongly against Zn(II) but not Co(II); however, *cnr* is only mildly upregulated by Co(II) compared with Ni(II) (70). In *C. metallidurans* CH34 wild type, the CzcCBA efflux pump keeps the periplasmic Co(II) level low, even in medium with a low metal content (75), so that CnrCBA is only produced at high (low mM) nickel, or even higher cobalt concentrations (5, 76).

In comparison to Ni(II), Co(II) has only seven electrons in the 3d orbital, six in the non-bonding d orbitals and one in an anti-bonding d-orbital. Octahedral complexes are possible, with a switch between the formal Co(II) and Co(III) oxidation states allowing the binding of the 6th beta-ligand or weakening of this bond, as for instance in cobalamin during mutase reactions (77). As outlined elsewhere (7), this provides low-spin Co(III) complexes with a low energetic state due to the half-filled 3d orbitals so that Co(III) complexes are kinetically stable, which traps cobalt in cobalamin complexes so that most of the cell-bound cobalt may reside in these complexes. Derivatives of cobalamin are even used to exchange cobalt between cells, allowing them to keep the concentration of unbound Co(II) in the cytoplasm very low (7).

Trapping of cobalt in cobalamin complexes may lower the concentration of Co(II) available for metalation of CobW3 and other proteins, so that Zn(II) may out-compete cobalt here (41). Indeed, *Pseudomonas denitrificans* strains can be used to produce up to 200 mg/L B₁₂ under biotechnological conditions (78). This would calculate to about 150 nM of B₁₂ in the growth medium, which would need the same Co(II) concentration to allow biosynthesis. *C. metallidurans* contains the genes for cobalamin biosynthesis or uptake; the respective proteins are there, but none of the genes was up- or down-regulated in *C. metallidurans* strain AE104 under metal stress or starvation conditions (79, 80). Although the abundance of the proteins involved in cobalamin biosynthesis seem not to be regulated under conditions of changing metal availability, product removal by trapping may increase the ratio of cytoplasmic Co bound to cobalamin. On the other hand, none of the tested strains exhausted the cobalt content of the growth medium. That would be expected if a strong cobalamin biosynthesis rate traps all the available cobalt in the center of B₁₂. At this stage, it cannot be concluded how much of the cytoplasmic cobalt is trapped as B₁₂ and how this trapping influences binding of Co(II) to CobW3 or the F_oE₁IBs (41).

CobW3 bound Zn(II), Ni(II), Co(II), and Cd(II), and each metal should form different complexes by binding to the variety of amino acid residues in the large C-terminal His-rich loop of the protein (Fig. S1). This may allow CobW3 to form a variety of conformations of its C-terminal domain, resulting in different actions of CobW3, for instance, during protein-protein interactions. Although Cd(II) should be exported by the P_{B₁₂}-type ATPases ZntA and CadA (15), *C. metallidurans* cells contain Ni-hydrogenases and maturation proteins like HypB, another member of the COG0523 protein family like the CobWs, even under heterotrophic growth conditions (5), and these proteins should serve as sinks for Ni(II). Therefore, only Co(II) remains to occupy Zn-binding sites and protect them from being bound by Cd(II). To prevent cobalt toxicity, however, the cellular Co(II) level has to be strictly controlled, which is accomplished by the interaction of CobW3, ZupT, DmeF and CobW2 (Fig. S1), and possibly trapping of Co(II) in cobalamin complexes.

MATERIALS AND METHODS

Bacterial strains and growth conditions

Strains used for experiments were derivatives of the plasmid-free derivative AE104 of *C. metallidurans* CH34 (5) and are listed in Table S2. Tris-buffered mineral salts medium (5) containing 2 g sodium gluconate/l (TMM) was used to cultivate these strains aerobically with shaking at 30°C. Modified versions of the standard TMM contained different zinc and magnesium concentrations (Table S1). Solid Tris-buffered media contained 20 g agar/L.

Dose-response growth curves in 96-well plates

Experiments were conducted in TMM. A pre-culture was incubated at 30°C, 200 rpm up to early stationary phase, then diluted 1:20 into fresh medium and incubated for 24 h at 30°C and 200 rpm. Overnight cultures were used to inoculate parallel cultures with increasing metal concentrations in 96-well plates (Greiner). Cells were cultivated for

25 h at 30°C and 1,300 rpm in a neoLab Shaker DTS-2 (neoLab, Heidelberg, Germany) and the optical density was determined at 600 nm in a TECAN Infinite M Nano reader (Tecan Group Ltd., Männedorf, Switzerland) as indicated. To calculate the IC_{50} values (inhibitory concentration: metal concentration that led to turbidity reduction by half) and the corresponding b -value (measure of the slope of the sigmoidal dose–response curve), the data were adapted to the formula $OD(c) = OD_0 / \{1 + \exp((c - IC_{50})/b)\}$, which is a simplified version of a Hill-type equation as introduced by Pace and Scholtz (81) as published (82). $OD(c)$ is the turbidity at a given metal concentration, OD_0 that had no added metal, and c is the metal concentration.

Time-dependent growth curves in 48-well plate

Experiments were conducted in TMM. A pre-culture was incubated at 30°C, 200 rpm up to early stationary phase, then diluted 1:20 into fresh medium and incubated for 24 h at 30°C and 200 rpm. Overnight cultures were diluted 50-fold in fresh medium with or without additions in 48-well plates (TPP). The kinetic loop consisted of 90 cycles and was performed in TECAN Spark microplate reader (TECAN, Switzerland). Shaking duration was 2,000 seconds, in orbital mode with an amplitude of 4 mm and frequency of 150 rpm. Optical density was measured at 600 nm at the end of each cycle.

Genetic techniques

Standard molecular genetic techniques were used (83, 84). For conjugative gene transfer, overnight cultures of donor strain *E. coli* S17/1 (85) and of the *C. metallidurans* recipient strains grown at 30°C in Tris- buffered medium were mixed (1:1) and plated onto nutrient broth agar. After 2 d, the bacteria were suspended in TMM, diluted, and plated onto selective media as previously described (83). Primer sequences are provided in Table S2.

Gene deletions

Primer sequences are also provided in Table S2. Plasmid pECD1002, a derivative of plasmid pCM184 (86), was used to construct deletion mutants. These plasmids harbor a kanamycin resistance cassette flanked by *loxP* recognition sites. Plasmid pECD1002 additionally carries alterations of 5 bp at each *loxP*-site. Using these mutant *loxP* sequences, multiple gene deletions within the same genome are possible without interferences by secondary recombination events (87, 88). Fragments of 300 bp upstream and downstream of the target gene were amplified by PCR, cloned into vector pGEM T-Easy (Promega), sequenced, and further cloned into plasmid pECD1002. The resulting plasmids were used in a double-crossover recombination in *C. metallidurans* strains to replace the respective target gene by the kanamycin-resistance cassette, which was subsequently also deleted by transient introduction of *cre* expression plasmid pCM157 (86). Cre recombinase is a site-specific recombinase from the phage P1 that catalyzes the *in vivo* excision of the kanamycin resistance cassette at the *loxP* recognition sites. The correct deletions of the respective transporter genes were verified by Southern DNA-DNA hybridization. For construction of multiple deletion strains, these steps were repeated. The resulting mutants carried a small open reading frame instead of the wild-type gene to prevent polar effects.

Inductively-coupled plasma mass spectrometry (ICP-MS)

Cells were incubated in TMM for 20 h at 30°C with shaking at 200 rpm, diluted 20-fold into fresh TMM medium, and shaking was continued at 30°C for 24 h. Cells were diluted 66-fold into fresh medium until 100 Klett was reached (mid-exponential phase of growth). Metals were added, and the cells were left growing until they reached 150 Klett. Ten milliliters of the cells were harvested by centrifugation, washed twice with 50 mM TrisHCl buffer (pH 7.0) containing 10 mM EDTA, and 150 mM NaCl at 4°C. For ICP-MS analysis, HNO₃ (trace metal grade; Normatom/PROLABO) was added to the samples to a final concentration of 67% (wt/vol), and the mixture was mineralized at

70°C for 2 h. Samples were diluted to a final concentration of 2% (wt/vol) nitric acid. Indium and germanium were added as internal standards at a final concentration of 1 ppb and 10 ppb each. Elemental analysis was performed via ICP-MS using Cetac ASX-560 sampler (Teledyne, Cetac Technologies, Omaha, Nebraska), a MicroFlow PFA-100 nebulizer (Elemental Scientific, Mainz, Germany), and an ICAP-RQ ICP-MS instrument (Thermo Fisher Scientific, Bremen) operating with a collision cell and flow rates of $4.5 \text{ mL} \times \text{min}^{-1}$ of He/H₂ [93%/7% (89)], with an Ar carrier flow rate of $0.76 \text{ L} \times \text{min}^{-1}$ and an Ar make-up flow rate at $15 \text{ L} \times \text{min}^{-1}$. An external calibration curve was recorded with ICP-multi-element standard solution XVI (Merck) in 2% (vol/vol) nitric acid. The sample was introduced via a peristaltic pump and analyzed for its metal content. For blank measurement and quality/quantity thresholds, calculations based on DIN32645 TMM were used. The results were calculated from the ppb data as atoms per cell as described (8).

Pulse-chase experiments with radioactive ⁶⁵Zn

Cells were incubated in TMM for 17 h at 30°C shaking at 200 rpm, diluted 20-fold into a second pre-culture in the medium that was used for the subsequent main culture (TMM, aZn, lZn, and lZn_lMg) and incubated with shaking at 30°C for 24 h. Cells were diluted 50-fold into the main culture, which was incubated with shaking at 30°C at 200 rpm until a turbidity of 150 Klett units was reached (mid-exponential phase of growth). The cells were harvested by centrifugation at 4°C, washed in the same volume of 10 mM TrisHCl (pH 7), suspended in the same volume of 10 mM TrisHCl (pH 7), and kept on ice until needed during the same day. For the experiments, sodium gluconate was added to 6 mL of the cell suspension to a final concentration of 2 g/L directly before the start. At $t = 0$, radioactive ⁶⁵Zn was added to the cell suspension to a final concentration of 1 μM Zn(II) and 60 nCi/mL. The ⁶⁵ZnCl₂ was supplied by POLATOM (certificate 022-106722-03622-0001).

The cells were incubated with shaking at 30°C. At 0.25, 5, 10, and 15 min, samples of 500 μL were removed and filtered through a membrane filter (0.2-μm pore size, Whatman cellulose nitrate membrane filters, Cytiva) using a vacuum-driven uptake apparatus. The samples were rapidly washed twice with 5 mL of 50 mM TrisHCl (pH 7) containing 50 mM EDTA. The activity was counted in a Liquid Scintillation Counter (PerkinElmer Tri-Carb 2810 TR) using Ultima Gold (PerkinElmer). The samples were counted twice for 2 min in a window from 0 to 200 keV.

For the chase, non-radioactive zinc was added at $t = 20$ min to a final concentration of 100 μM. Incubation was continued with shaking at 30°C, and samples were removed at 20.25, 25, 30, 35, and 40 min. They were treated and analyzed as described above for the samples of the uptake period.

A sample of 100 μL was counted to determine the total radioactivity of the ⁶⁵Zn in the cell suspension used for the pulse-chase experiment. From this value, the mol zinc per cpm ratio was derived. For each time sample, the mean value and technical deviation of the two 2 min counts were calculated. Two zero controls were subtracted, one for the background radioactivity at the time of the experiment and one for the chemical adsorption of ⁶⁵Zn by the membrane filter. The resulting value was multiplied with the mol/cpm ratio of the respective experiment to give the mol ⁶⁵Zn per 500 μL time sample. The actual cell number in the sample had been determined via an equilibration curve for the turbidity at 600 nm, so that the mol ⁶⁵Zn per cell and subsequently the number of the ⁶⁵Zn atoms per cell could be calculated.

All experiments were performed at least three times. For each individual experiment, the zinc content per cell at 7.5 min was calculated from the 5 min and 10 min values. This value was used to correct the number of atoms per cell for all experiments involving the same mutant and the same growth condition. Experiments with large correction factors were removed and the respective experiment repeated. For each strain and condition, the mean values and deviations of the ⁶⁵Zn atoms per cell were finally calculated. This

value was designated as the cellular metal content $C(t)$ for the respective mutant and growth condition.

Pulse-chase with ^{65}Zn measured: (i) the initial zinc uptake velocity $v_{\text{up}}(0)$ at $t = 0$; (ii) the cellular ^{65}Zn content C_{20} at the end of the uptake period (time point represented in Fig. 2 by the horizontal bar); (iii) the extrapolated maximum zinc content after the uptake period C_{max} ; (iv) the efflux velocity v_{eff} at the beginning of the chase at 20 min; (v) the corresponding initial zinc content C_0 used to calculate v_{eff} ; and (vi) and the final zinc content C_{40} at the end of the chase period (Fig. 2, $t = 40$ min). To obtain these data, the uptake phase up to 20 min of the pulse-chase experiment was adapted to the equation $C(t) = C_{\text{max}} \cdot t / (K_t + t)$ using the Lineweaver-Burk-like plot $1 / C(t) = 1 / C_{\text{max}} + K_t / C_{\text{max}} \cdot 1 / t$. The first deviation by time of the equation $C(t) = C_{\text{max}} \cdot t / (K_t + t)$ was $dC(t)/dt = C_{\text{max}} \cdot K_t / (K_t + t)^2$. At $t = 0$, this gave the initial uptake rate $v_{\text{up}}(0) = C_{\text{max}} / K_t$. After the chase after 20 min, the cell-bound zinc content was modeled by the decay function $C(t) = C_0 \cdot e^{-(t \cdot \tau)}$ using the plot $\ln C(t) = \ln C_0 - t \cdot \tau$. The first deviation by time of the equation $C(t) = C_0 \cdot e^{-(t \cdot \tau)}$ was $dC(t)/dt = -\tau \cdot C_0 \cdot e^{-(t \cdot \tau)}$. However, at $t = 0$, this value was the initial net efflux rate $v_{\text{eff}}(0) = -\tau \cdot C_0$. In contrast to the initial uptake rate that was no net rate because the cells did not contain ^{65}Zn at $t = 0$, $v_{\text{eff}}(0)$ was a net rate, and the result of the real efflux rate after chase minus the rate of ^{65}Zn re-import at this time.

Experiments with stable ^{67}Zn

Stable enriched ^{67}Zn was employed to determine (vii) the resident zinc pool (ZP) ZP1 at the beginning of the experiment; (viii) the zinc pools ZP1 and ZP2 after the uptake period; and (ix) finally, these pools ZP1 and ZP2 after the chase period. The cell suspensions were prepared in the respective media as described for the pulse-chase experiments above; however, the respective growth medium was used instead of uptake buffer for these experiments. After a zero sample had been removed for the ICP-MS analysis, isotope-enriched $^{67}\text{Zn}(\text{II})$ was added to a final concentration of $1 \mu\text{M}$. Incubation was continued with shaking for 20 min, a sample was removed, and the remaining cells were chased with non-enriched $\text{Zn}(\text{II})$ added at a final concentration of $100 \mu\text{M}$. Incubation was continued for 20 min with shaking at 30°C , and the third sample was removed. The cells in the respective samples were harvested by centrifugation, washed twice with 50 mM TrisHCl buffer (pH 7.0) containing 50 mM EDTA at 0°C , suspended in 50 mM TrisHCl buffer (pH 7.0), and mineralized for the subsequent ICP-MS analysis. The ^{67}Zn (94% ^{67}Zn) was provided as metal from Nakima Ltd (Savyon, Israel) and oxidized using HCl on ice. The zinc content was verified by ICP-MS.

For the calculation of different zinc pools in the cells, the ratio of ^{67}Zn in the isotope-enriched zinc solution (94%) and non-enriched "usual" zinc [4.1% (90)] was used. The ICP-MS measurement calculates the quantity of an element from that of its isotopes, thereby correcting for the % of the natural abundance of the respective isotope. The zinc pool 1 (ZP1) was defined as the cellular zinc pool before addition of isotope-enriched ^{67}Zn and was equal to the ^{64}Zn ICP-MS result [natural abundance 48.6% (90)]. Similar results were obtained by using ^{66}Zn (27.9%) instead of ^{65}Zn . Zinc pool 2 (ZP2) was the zinc pool after incubation of the cells with ^{67}Zn . ZP2 was the ^{67}Zn value coming from the ICP-MS (corrected for a natural abundance 4.1%) minus the ^{64}Zn value (0.75% in the ^{67}Zn -enriched zinc solution) and the result was divided by 22.2346.

Statistics

Students' t -test was used, but in most cases, the distance (D) value, D, has been used several times previously for such analyses (10, 91, 92). It is a simple, more useful value than Student's t -test because non-intersecting deviation bars of two values ($D > 1$) for three repeats always mean a statistically relevant ($\geq 95\%$) difference, provided the deviations are within a similar range. At $n = 4$, significance is $\geq 97.5\%$, at $n = 5 \geq 99\%$ (significant), and at $n = 8 \geq 99.9\%$ (highly significant).

ACKNOWLEDGMENTS

Funding for this work was provided by the Deutsche Forschungsgemeinschaft (Ni262/19).

We thank Gary Sawers for critically reading the manuscript and Grit Schleuder for expert technical support.

AUTHOR AFFILIATIONS

¹Molecular Microbiology, Institute for Biology/Microbiology, Martin-Luther-University Halle-Wittenberg, Halle (Saale), Germany

²Department of Environmental Analytical Chemistry, Helmholtz Centre for Environmental Research – UFZ, Leipzig, Germany

AUTHOR ORCID*s*

Dietrich H. Nies  <http://orcid.org/0000-0002-4516-8267>

FUNDING

Funder	Grant(s)	Author(s)
Deutsche Forschungsgemeinschaft (DFG)	NI262/19-2	Dietrich H. Nies

ADDITIONAL FILES

The following material is available [online](#).

Supplemental Material

Supplemental material (JB00226-24-s0001.pdf), Tables S1 to S5; Figures S1 to S7.

REFERENCES

- Janssen PJ, Morin N, Mergeay M, Leroy B, Wattiez R, Vallaeys T, Waleron K, Waleron M, Wilmotte A, Quillardet P, de Marsac NT, Talla E, Zhang C-C, Leys N. 2010. Genome sequence of the edible *Cyanobacterium arthrospira* sp. PCC 8005. *J Bacteriol* 192:2465–2466. <https://doi.org/10.1128/JB.00116-10>
- Diels L, Mergeay M. 1990. DNA probe-mediated detection of resistant bacteria from soils highly polluted by heavy metals. *Appl Environ Microbiol* 56:1485–1491. <https://doi.org/10.1128/aem.56.5.1485-1491.1990>
- Stiers M, Mergeay M, Pinson H, Janssen L, Voets E, De Cauwer H, Schepens T. 2021. Individualized mechanical ventilation in a shared ventilator setting: limits, safety and technical details. *J Clin Monit Comput* 35:1299–1309. <https://doi.org/10.1007/s10877-020-00596-7>
- Reith F, Rogers SL, McPhail DC, Webb D. 2006. Biomineralization of gold: biofilms on bacterioform gold. *Science* 313:233–236. <https://doi.org/10.1126/science.1125878>
- Mergeay M, Nies D, Schlegel HG, Gerits J, Charles P, Van Gijsegem F. 1985. *Alcaligenes eutrophus* CH34 is a facultative chemolithotroph with plasmid-bound resistance to heavy metals. *J Bacteriol* 162:328–334. <https://doi.org/10.1128/jb.162.1.328-334.1985>
- diCenzo GC, Finan TM. 2017. The divided bacterial genome: structure, function, and evolution. *Microbiol Mol Biol Rev* 81:e00019-17. <https://doi.org/10.1128/MMBR.00019-17>
- Nies DH. 2016. The biological chemistry of the transition metal "Transportome" of *Cupriavidus metallidurans*. *Metallomics* 8:481–507. <https://doi.org/10.1039/c5mt00320b>
- Kirsten A, Herzberg M, Voigt A, Seravalli J, Grass G, Scherer J, Nies DH. 2011. Contributions of five secondary metal uptake systems to metal homeostasis of *Cupriavidus metallidurans* CH34. *J Bacteriol* 193:4652–4663. <https://doi.org/10.1128/JB.05293-11>
- Herzberg M, Bauer L, Kirsten A, Nies DH. 2016. Interplay between seven secondary metal transport systems is required for full metal resistance of *Cupriavidus metallidurans*. *Metallomics* 8:313–326. <https://doi.org/10.1039/c5mt00295h>
- Große C, Wolff-Menzler C. 2016. Analysis and assessment of modifications of the PEPP system introduced by the PEPP catalogue 2015. *Gesundheitswesen* 78:446–451. <https://doi.org/10.1055/s-0035-1548850>
- Busch W, Saier MHJ. 2002. The transporter classification (TC) system. *Crit Rev Biochem Mol Biol* 37:287–337. <https://doi.org/10.1080/10409230290771528>
- Saier MHJ, Tran CV, Barabote RD. 2006. TCDB: the transporter classification database for membrane transport protein analyses and information. *Nucleic Acids Res* 34:D181–D186. <https://doi.org/10.1093/nar/gkj001>
- Abelson PH, Aldous E. 1950. Ion antagonisms in microorganisms – interference of normal magnesium metabolism by nickel, cobalt, cadmium, zinc, and manganese. *J Bacteriol* 60:401–413. <https://doi.org/10.1128/jb.60.4.401-413.1950>
- Nelson DL, Kennedy EP. 1971. Magnesium transport in *Escherichia coli* – inhibition by cobaltous ion. *J Biol Chem* 246:3042–3049.
- Scherer J, Nies DH. 2009. CzcP is a novel efflux system contributing to transition metal resistance in *Cupriavidus metallidurans* CH34. *Mol Microbiol* 73:601–621. <https://doi.org/10.1111/j.1365-2958.2009.06792.x>
- Munkelt D, Grass G, Nies DH. 2004. The chromosomally encoded cation diffusion facilitator proteins DmeF and FieF from *Wautersia metallidurans* CH34 are transporters of broad metal specificity. *J Bacteriol* 186:8036–8043. <https://doi.org/10.1128/JB.186.23.8036-8043.2004>
- Herzberg M, Dobritzsch D, Helm S, Baginsky S, Nies DH. 2014. The zinc repository of *Cupriavidus metallidurans*. *Metallomics* 6:2157–2165. <https://doi.org/10.1039/c4mt00171k>
- Nies DH, Schleuder G, Galea D, Herzberg DH. 2024. A flow equilibrium of zinc in cells of *Cupriavidus metallidurans*. *J Bacteriol* 206:e00080-24. <https://doi.org/10.1128/jb.00395-23>

19. Schmidt C, Schwarzenberger C, Große C, Nies DH. 2014. Furc regulates expression of *zupT* for the central zinc importer *zupT* of *Cupriavidus metallidurans*. *J Bacteriol* 196:3461–3471. <https://doi.org/10.1128/JB.01713-14>
20. Bütof L, Große C, Lilie H, Herzberg M, Nies DH. 2019. Interplay between the zur regulon components and metal resistance in *Cupriavidus metallidurans*. *J Bacteriol* 201:e00192-19. <https://doi.org/10.1128/JB.00192-19>
21. Bütof L, Schmidt-Vogler C, Herzberg M, Große C, Nies DH. 2017. The components of the unique zur regulon of *Cupriavidus metallidurans* mediate cytoplasmic zinc handling. *J Bacteriol* 199:e00372-17. <https://doi.org/10.1128/JB.00372-17>
22. Chen YY, O'Halloran TV. 2022. A zinc chaperone mediates the flow of an inorganic commodity to an important cellular client. *Cell* 185:2013–2015. <https://doi.org/10.1016/j.cell.2022.05.012>
23. Maret W. 2022. Escort proteins for cellular zinc ions. *Nature* 608:38–39. <https://doi.org/10.1038/d41586-022-01988-2>
24. Haas CE, Rodionov DA, Kropat J, Malasarn D, Merchant SS. 2009. A subset of the diverse COG0523 family of putative metal chaperones is linked to zinc homeostasis in all kingdoms of life. *BMC Genomics* 10:470. <https://doi.org/10.1186/1471-2164-10-470>
25. Schulz V, Galea D, Herzberg M, Nies DH. 2024. Protecting the Achilles heel: three Fole_I-type GTP-cyclohydrolases needed for full growth of metal resistant *Cupriavidus metallidurans* under a variety of conditions. *J Bacteriol* 206
26. Nies DH. 2019. The ancient alarmone ZTP and zinc homeostasis in *Bacillus subtilis*. *Mol Microbiol* 112:741–746. <https://doi.org/10.1111/mmi.14332>
27. Chandransu P, Huang X, Gaballa A, Helmann JD. 2019. *Bacillus subtilis* fole is sustained by the ZagA zinc Metallochaperone and the alarmone ZTP under conditions of zinc deficiency. *Mol Microbiol* 112:751–765. <https://doi.org/10.1111/mmi.14314>
28. Sankaran B, Bonnett SA, Shah K, Gabriel S, Reddy R, Schimmel P, Rodionov DA, Helmann JD, Iwata-Reuyl D, Swairjo MA. 2009. Zinc-independent folate biosynthesis: genetic, biochemical, and structural investigations reveal new metal dependence for GTP cyclohydrolase IB. *J Bacteriol* 191:6936–6949. <https://doi.org/10.1128/JB.00287-09>
29. Roux M, Covés J. 2002. The iron-containing superoxide dismutase of *Ralstonia metallidurans* CH34. *FEMS Microbiol Lett* 210:129–133. <https://doi.org/10.1111/j.1574-6968.2002.tb11171.x>
30. Braun V, Hantke K. 2007. Acquisition of iron by bacteria, p 189–217. In Nies DH, Silver S (ed), *Molecular Microbiology of heavy metals*. Vol. 6. Springer-Verlag, Berlin-Heidelberg.
31. Massey V, Strickland S, Mayhew SG, Howell LG, Engel PC, Matthews RG, Schuman M, Sullivan PA. 1969. The production of superoxide anion radicals in the reaction of reduced flavins and flavoproteins with molecular oxygen. *Biochem Biophys Res Commun* 36:891–897. [https://doi.org/10.1016/0006-291x\(69\)90287-3](https://doi.org/10.1016/0006-291x(69)90287-3)
32. Haber F, Weiss J. 1932. Über die katalyse des hydroperoxydes. *Naturwissenschaften* 20:948–950. <https://doi.org/10.1007/BF01504715>
33. Liochev SI, Fridovich I. 2002. The haber-weiss cycle - 70 years later: an alternative view. *Redox Rep.* 7:55–57; <https://doi.org/10.1179/135100002125000190>
34. Fazio TG, Roth JR. 1996. Evidence that the CysG protein catalyzes the first reaction specific to B-12 synthesis in *Salmonella typhimurium*, insertion of cobalt. *J Bacteriol* 178:6952–6959. <https://doi.org/10.1128/jb.178.23.6952-6959.1996>
35. Ranquet C, Ollagnier-de-Choudens S, Loiseau L, Barras F, Fontecave M. 2007. Cobalt stress in *Escherichia coli*. *J Bio Chem* 282:30442–30451. <https://doi.org/10.1074/jbc.M702519200>
36. Thorgersen MP, Downs DM. 2007. Cobalt targets multiple metabolic processes in *Salmonella enterica*. *J Bacteriol* 189:7774–7781. <https://doi.org/10.1128/JB.00962-07>
37. Fantino JR, Py B, Fontecave M, Barras F. 2010. A genetic analysis of the response of *Escherichia coli* to cobalt stress. *Environ Microbiol* 12:2846–2857. <https://doi.org/10.1111/j.1462-2920.2010.02265.x>
38. Ammendola S, Ciavardelli D, Consalvo A, Battistoni A. 2020. Cobalt can fully recover the phenotypes related to zinc deficiency in *salmonella typhimurium*. *Metallomics* 12:2021–2031. <https://doi.org/10.1039/d0mt00145g>
39. Irving H, Williams RJP. 1948. Order of stability of metal complexes. *Nature* 162:746–747. <https://doi.org/10.1038/162746a0>
40. Osman D, Robinson NJ. 2023. Protein metalation in a nutshell. *FEBS Lett* 597:141–150. <https://doi.org/10.1002/1873-3468.14500>
41. Young TR, Martini MA, Foster AW, Glasfeld A, Osman D, Morton RJ, Deery E, Warren MJ, Robinson NJ. 2021. Calculating metalation in cells reveals CobW ACQUIRES Co(II) for vitamin B(12) biosynthesis while related proteins prefer Zn(II). *Nat Commun* 12:1195. <https://doi.org/10.1038/s41467-021-21479-8>
42. Pfennig N. 1974. *Rhodospseudomonas globiformis*, Sp-N, a new species of *Rhodospirillaceae*. *Arch Microbiol* 100:197–206. <https://doi.org/10.1007/BF00446317>
43. Herzberg M, Bauer L, Nies DH. 2014. Deletion of the *zupT* gene for a zinc importer influences zinc pools in *Cupriavidus metallidurans* CH34. *Metallomics* 6:421–436. <https://doi.org/10.1039/c3mt00267e>
44. Schulz V, Schmidt-Vogler C, Strohmeier P, Weber S, Kleemann D, Nies DH, Herzberg M. 2021. Behind the shield of czc: ZntR controls expression of the gene for the zinc-exporting P-type ATPase ZntA in *Cupriavidus metallidurans*. *J Bacteriol* 203:e00052-21. <https://doi.org/10.1128/JB.00052-21>
45. Grass G, Otto M, Fricke B, Haney CJ, Rensing C, Nies DH, Munkelt D. 2005. Fief (Yif) from *Escherichia coli* mediates decreased cellular accumulation of iron and relieves iron stress. *Arch Microbiol* 183:9–18. <https://doi.org/10.1007/s00203-004-0739-4>
46. Helbig K, Grosse C, Nies DH. 2008. Cadmium toxicity in glutathione mutants of *Escherichia coli*. *J Bacteriol* 190:5439–5454. <https://doi.org/10.1128/JB.00272-08>
47. Helbig K, Bleuel C, Krauss GJ, Nies DH. 2008. Glutathione and transition metal homeostasis in *Escherichia coli*. *J Bacteriol* 190:5431–5438. <https://doi.org/10.1128/JB.00271-08>
48. Wang ZJ, Zhang Y, Chen YH, Han FY, Shi YX, Pan S, Li Z. 2024. Competition of Cd(II) and Pb(II) on the bacterial cells: a new insight from bioaccumulation based on nanosims imaging. *Appl Environ Microbiol* 90. <https://doi.org/10.1128/aem.01453-23>
49. Cornejo FA, Muñoz-Villagrán C, Luraschi RA, Sandoval-Díaz MP, Cancino CA, Pugin B, Morales EH, Piotrowski JS, Sandoval JM, Vásquez CC, Arenas FA. 2023. Soft-metal(loid)s induce protein aggregation in *Escherichia coli*. *Front Microbiol* 14. <https://doi.org/10.3389/fmicb.2023.1281058>
50. Begg SL, Eijkelkamp BA, Luo Z, Couñago RM, Morey JR, Maher MJ, Ong C-LY, McEwan AG, Kobe B, O'Mara ML, Paton JC, McDevitt CA. 2015. Dysregulation of transition metal ion homeostasis is the molecular basis for cadmium toxicity in *Streptococcus pneumoniae*. *Nat Commun* 6:6418. <https://doi.org/10.1038/ncomms7418>
51. Wang AY, Crowley DE. 2005. Global gene expression responses to cadmium toxicity in *Escherichia coli*. *J Bacteriol* 187:3259–3266. <https://doi.org/10.1128/JB.187.9.3259-3266.2005>
52. Nies DH. 2022. Edited by C. J. Hurst. *Microbial metabolism of metals and metalloids*, Vol. 10, p 21–52. Vol. 10. Springer, Heidelberg.
53. Nies DH. 2022. How is a zinc ion correctly allocated to a zinc-dependent protein?, p 579–659. In Hurst CJ (ed), *Microbial metabolism of metals and metalloids*. Vol. 10. Springer, Heidelberg.
54. Weiss A, Murdoch CC, Edmonds KA, Jordan MR, Monteith AJ, Perera YR, Rodríguez Nassif AM, Petoletti AM, Beavers WN, Munneke MJ, Drury SL, Krystofiak ES, Thalluri K, Wu H, Kruse ARS, DiMarchi RD, Caprioli RM, Spraggins JM, Chazin WJ, Giedroc DP, Skaar EP. 2022. Zn-regulated GTPase metalloprotein activator 1 modulates vertebrate zinc homeostasis. *Cell* 185:2148–2163. <https://doi.org/10.1016/j.cell.2022.04.011>
55. Pasquini M, Grosjean N, Hixson KK, Nicora CD, Yee EF, Lipton M, Blaby IK, Haley JD, Blaby-Haas CE. 2022. Zng1 is a GTP-dependent zinc transferase needed for activation of methionine aminopeptidase. *Cell Rep* 39:110834. <https://doi.org/10.1016/j.celrep.2022.110834>
56. Sydor AM, Jost M, Ryan KS, Turo KE, Douglas CD, Brennan CL, Zamble DB. 2013. Metal binding properties of *Escherichia coli* YjiA, a member of the metal homeostasis-associated COG0523 family of GTPases. *Biochemistry* 52:1788–1801. <https://doi.org/10.1021/bi301600z>
57. Krężel A, Maret W. 2016. The biological inorganic chemistry of zinc ions. *Arch Biochem Biophys* 611:3–19. <https://doi.org/10.1016/j.abb.2016.04.010>
58. Housecroft CE, Constable EC. 2006. *Chemistry (Weinheim an der Bergstrasse, Germany)*. 3rd ed. Pearson Education Limited, Essex, England.

59. Markov D, Naryshkina T, Mustaev A, Severinov K. 1999. A zinc-binding site in the largest subunit of DNA-dependent RNA polymerase is involved in enzyme assembly. *Genes Dev* 13:2439–2448. <https://doi.org/10.1101/gad.13.18.2439>
60. Huang WJ, Sinclair RB, Powers L. 1992. The structure of the zinc sites of *Escherichia coli* DNA-dependent RNA polymerase. *J Biol Chem* 267:25560–25567. [https://doi.org/10.1016/S0021-9258\(19\)74077-0](https://doi.org/10.1016/S0021-9258(19)74077-0)
61. Rebelo J, Auerbach G, Bader G, Bracher A, Nar H, Hösl C, Schramek N, Kaiser J, Bacher A, Huber R, Fischer M. 2003. Biosynthesis of pteridines. reaction mechanism of GTP cyclohydrolase I. *J Mol Biol* 326:503–516. [https://doi.org/10.1016/s0022-2836\(02\)01303-7](https://doi.org/10.1016/s0022-2836(02)01303-7)
62. Auerbach G, Herrmann A, Bracher A, Bader G, Gütllich M, Fischer M, Neukamm M, Garrido-Franco M, Richardson J, Nar H, Huber R, Bacher A. 2000. Zinc plays a key role in human and bacterial GTP cyclohydrolase I. *Proc Natl Acad Sci U S A* 97:13567–13572. <https://doi.org/10.1073/pnas.240463497>
63. Debye P, Hückel E. 1923. Zur Theorie der Elektrolyte I. Gefrierpunktserniedrigung und verwandte Erscheinungen. *Physikal Zeitschr* 24:185–206.
64. Hensley MP, Tierney DL, Crowder MW. 2011. Zn(II) binding to *Escherichia coli* 70s ribosomes. *Biochemistry* 50:9937–9939. <https://doi.org/10.1021/bi200619w>
65. Layer G, Ollagnier-de Choudens S, Sanakis Y, Fontecave M. 2006. Iron-sulfur cluster biosynthesis: characterization of *Escherichia coli* CyaY as an iron donor for the assembly of [2Fe-2S] clusters in the scaffold IscU. *J Biol Chem* 281:16256–16263. <https://doi.org/10.1074/jbc.M513569200>
66. Hirth N, Gerlach M-S, Wiesemann N, Herzberg M, Große C, Nies DH. 2023. Full copper resistance in *Cupriavidus metallidurans* requires the interplay of many resistance systems. *Appl Environ Microbiol* 89:e0056723. <https://doi.org/10.1128/aem.00567-23>
67. Liesegang H. 1993. Characterization of the inducible nickel and cobalt resistance determinant *cnr* from pMOL28 of *Alcaligenes eutrophus* CH34. *J Bacteriol* 175:767–778. <https://doi.org/10.1128/jb.175.3.767-778.1993>
68. Tibazarwa C, Wuertz S, Mergeay M, Wyns L, van Der Lelie D. 2000. Regulation of the *cnr* cobalt and nickel resistance determinant of *Ralstonia eutropha* (*Alcaligenes eutrophus*) CH34. *J Bacteriol* 182:1399–1409. <https://doi.org/10.1128/JB.182.5.1399-1409.2000>
69. Grass G, Fricke B, Nies DH. 2005. Control of expression of a periplasmic nickel efflux pump by periplasmic nickel concentrations. *Biometals* 18:437–448. <https://doi.org/10.1007/s10534-005-3718-6>
70. Grass G, Grosse C, Nies DH. 2000. Regulation of the *cnr* cobalt/nickel resistance determinant from *Ralstonia* sp. CH34. *J Bacteriol* 182:1390–1398. <https://doi.org/10.1128/JB.182.5.1390-1398.2000>
71. Pompidor G, Maillard AP, Girard E, Gambarelli S, Kahn R, Covès J. 2008. X-ray structure of the metal-sensor CnrX in both the apo- and copper-bound forms. *FEBS Lett* 582:3954–3958. <https://doi.org/10.1016/j.febslet.2008.10.042>
72. Trepreau J, Girard E, Maillard AP, de Rosny E, Petit-Haertlein I, Kahn R, Covès J. 2011. Structural basis for metal sensing by CnrX. *J Mol Biol* 408:766–779. <https://doi.org/10.1016/j.jmb.2011.03.014>
73. Maillard AP, Künnemann S, Große C, Volbeda A, Schleuder G, Petit-Haertlein I, de Rosny E, Nies DH, Covès J. 2015. Response of CnrX from *Cupriavidus metallidurans* CH34 to nickel binding. *Metallomics* 7:622–631. <https://doi.org/10.1039/c4mt00293h>
74. Trepreau J, Grosse C, Mouesca J-M, Saret G, Girard E, Petit-Haertlein I, Künnemann S, Desbourdes C, de Rosny E, Maillard AP, Nies DH, Covès J. 2014. Metal sensing and signal transduction by CnrX from *Cupriavidus metallidurans* CH34: role of the only methionine assessed by a functional, spectroscopic, and theoretical study. *Metallomics* 6:263–273. <https://doi.org/10.1039/c3mt00248a>
75. Schromm TM, Grosse CU. 2023. From 2D projections to the 3D rotation matrix: an attempt for finding a machine learning approach for the efficient evaluation of mechanical joining elements in X-ray computed tomography volume data. *SN Appl Sci* 5:18. <https://doi.org/10.1007/s42452-022-05220-8>
76. Nies DH, Rehbein G, Hoffmann T, Baumann C, Grosse C. 2006. Paralogs of genes encoding metal resistance proteins in *Cupriavidus metallidurans* strain CH34. *Microb Physiol* 11:82–93. <https://doi.org/10.1159/000092820>
77. Takahashi-Iñiguez T, García-Hernandez E, Arreguín-Espinosa R, Flores ME. 2012. Role of vitamin B12 on methylmalonyl-coA mutase activity. *J Zhejiang Univ Sci B* 13:423–437. <https://doi.org/10.1631/jzus.B1100329>
78. Xia W, Chen W, Peng W, Li K. 2015. Industrial vitamin B production by *Pseudomonas denitrificans* using maltose syrup and corn steep liquor as the cost-effective fermentation substrates. *Bioprocess Biosyst Eng* 38:1065–1073. <https://doi.org/10.1007/s00449-014-1348-5>
79. Große C, Kohl TA, Niemann S, Herzberg M, Nies DH. 2022. Loss of mobile genomic islands in metal resistant, hydrogen-oxidizing *Cupriavidus metallidurans*. *Appl Environ Microbiol* 88:e0204821. <https://doi.org/10.1128/AEM.02048-21>
80. Große C, Grau J, Große I, Nies DH. 2022. Importance of RpoD- and non-RpoD-dependent expression of horizontally acquired genes in *Cupriavidus metallidurans*. *Microbiol Spectr* 10:e0012122. <https://doi.org/10.1128/spectrum.00121-22>
81. Pace CN, Scholtz MJ. 1997. Edited by T. Creighton. Protein structure: a practical approach, p 299–322. IRL press, Oxford, UK.
82. Anton A, Weltrowski A, Haney CJ, Franke S, Grass G, Rensing C, Nies DH. 2004. Characteristics of zinc transport by two bacterial cation diffusion facilitators from *Ralstonia metallidurans* and *Escherichia coli*. *J Bacteriol* 186:7499–7507. <https://doi.org/10.1128/JB.186.22.7499-7507.2004>
83. Nies D, Mergeay M, Friedrich B, Schlegel HG. 1987. Cloning of plasmid genes encoding resistance to cadmium, zinc, and cobalt in *Alcaligenes eutrophus* CH34. *J Bacteriol* 169:4865–4868. <https://doi.org/10.1128/jb.169.10.4865-4868.1987>
84. Sambrook J, Fritsch EF, Maniatis T. 1989. Molecular cloning, a laboratory manual. 2nd ed. Cold Spring Harbor Laboratory, Cold Spring Harbor, N.Y.
85. Simon R, Priefer U, Pühler A. 1983. A broad host range mobilization system for *in vivo* genetic engineering: transposon mutagenesis in gram-negative bacteria. *Nat Biotechnol* 1:784–791. <https://doi.org/10.1038/nbt1183-784>
86. Marx CJ, Lidstrom ME. 2002. Broad-host-range *CRE-Lox* system for antibiotic marker recycling in Gram-negative bacteria. *Biotechniques* 33:1062–1067. <https://doi.org/10.2144/02335rr01>
87. Suzuki N, Nonaka H, Tsuge Y, Inui M, Yukawa H. 2005. New multiple-deletion method for the *Corynebacterium glutamicum* genome, using a mutant *Lox* sequence. *Appl Environ Microbiol* 71:8472–8480. <https://doi.org/10.1128/AEM.71.12.8472-8480.2005>
88. Albert H, Dale EC, Lee E. 1995. Site-specific integration of DNA into wild-type and mutant *Lox* sites placed in the plant genome. *Plant J* 7:649–659. <https://doi.org/10.1046/j.1365-313x.1995.7040649.x>
89. Wagegg W, Braun V. 1981. Ferric citrate transport in *Escherichia coli* requires outer membrane receptor protein FECA. *J Bacteriol* 145:156–163. <https://doi.org/10.1128/jb.145.1.156-163.1981>
90. Weast RC. 1984. CRC handbook of chemistry and physics. 64th ed. CRC Press, Inc., Boca Raton, Florida, USA.
91. Herzberg M, Schüttau M, Reimers M, Große C, Nies DH. 2015. Synthesis of nickel-iron hydrogenase in *Cupriavidus metallidurans* is controlled by metal-dependent silencing and UN-silencing of genomic islands. *Metallomics* 7:632–649. <https://doi.org/10.1039/c4mt00297k>
92. Wiesemann N, Mohr J, Grosse C, Herzberg M, Hause G, Reith F, Nies DH. 2013. Influence of copper resistance determinants on gold transformation by *Cupriavidus metallidurans* strain CH34. *J Bacteriol* 195:2298–2308. <https://doi.org/10.1128/JB.01951-12>